SYSTEM AND COMPONENT ANALYSIS OF A 1KW DIESEL FUELLED SOFC SYSTEM

by

Yasir Zaman Khan

A thesis submitted to the Department of Chemical Engineering

In conformity with the requirements for

the degree of Masters of Applied Science

Queen's University

Kingston, Ontario, Canada

(October, 2013)

Abstract

The first part of this thesis intends to create a fuel processor model capable of generating 1kW power as output through the use of a solid oxide fuel cell system. The fuel processor system consists of a reformer, heat exchanger network, desulphurizer and an afterburner. Modelled in VMGSim^{TM}, inlet diesel gas is provided at the mass flow rate of 0.2596kg/hour, with the oxygen to carbon ratio calculated at 0.31 and the steam to carbon ratio arbitrarily set to be 2.25. The diesel fuel is preheated and mixed with air and steam and then fed to the auto-thermal reformer. The higher hydrocarbons are broken down and converted into hydrogen. The outlet of the reformer is fed into the SOFC where H_2 is converted to generate energy which, in this case is approximately 1200W. The off gas is fed to the afterburner; where the remaining H_2 is burnt and the energy is used to provide for steam generation and pre-heating through the heat exchangers. The project also focuses upon performing basic sizing calculations on components of the system. The fuel cell efficiency was found to be 62% and the system efficiency was calculated to be approximately 41%, which falls within the range given in literature.

For the second part of this work, a ceramic porous tail-gas burner using a non-premixed feed of anode exhaust and air was modeled using COMSOL™. The reaction kinetics were experimentally assessed on the basis of COMSOL™ limitations and accuracy of the comparative results. Three performance metrics were evaluated in the analysis: i) velocity profile, ii) temperature profile, and iii) concentration profile. These metrics confirm the combustion reaction at the outer boundary of the porous ceramic in the burner. The spike of temperature and decrease of mass fraction of hydrogen, carbon monoxide and methane to approximately zero in the outlet exhaust confirms this study. This study was further validated by comparing results with the experimental data collected at NRC-IFCI. The results of COMSOL™ model agreed with the experimental results of NRC-IFCI.

Acknowledgements

Putting together a thesis of this calibre comes with its fair share of trials and tribulations. This note attempts to thank and acknowledge those people who kept me on track along the way. Although it cannot hold a candle to returning the impact they have had in my life, this is my attempt at showing some gratitude.

First and foremost I must thank my supervisor, friend, and mentor Dr. Brant A. Peppley. He has guided me when the path forward was uncertain, helped me through my times of weakness, and made sure my feet never left the ground in my times of victory. In the end he has helped me to produce a piece of work with the level of depth, analytical rigour, and quality of presentation. I did not think myself capable of. The completion of this thesis would simply not be possible without his involvement.

I would also like to thank Adam Tuck for his extraordinary level of knowledge and useful inputs in the design of SOFC fuel cell systems. Lab colleagues Rajesh Parmar (PhD.) and Mayur Mundhwa (PhD.) are certainly more talented than they know and never turned me away for any request for troubleshooting or general advice.

I'd like to thank my family for their unconditional love and support throughout this process. My brother Rashid Khan, for his stalwart mentality, and my parents, for never failing to check in on me. My friends Andrew Beshay and Mukund Chopra deserve some recognition for always helping to give me a laugh when I needed it most.

Also most importantly I must thank my nieces Leena Sara Khan and the recently arrived Ayra Jehan Khan for keeping me motivated to go on and contribute to a cleaner greener world for them. Without this intrinsic motivation, none of this would have been possible.

Table of Contents

List of Figures

List of Tables

Nomenclature

ε	extent of reaction [kmol/s]
ρ	density [kg/m^3]
μ	dynamic viscosity [kg/m.s]
η	effectiveness factor
κ	permeability [m^2/s]
ϕ	porosity
$\mathcal{S}/\mathcal{C}$	steam to carbon ratio
O_2/C	oxygen to carbon ratio
t	layer thickness [m]
T	temperature [K]
u	horizontal velocity [m/s]
V	vertical velocity [m/s]
U_f	fuel utilization in SOFC
U_a	air utilization in SOFC
v	diffusion volume [m^3]
i,j	component (e.g. CO, H2)
W	power [W]

x	axial coordinate
X	mole fraction
SOFC	Solid Oxide Fuel Cell
ṅCO	molar flow rate CO at anode feed [kgmol/s]
ṅ$CO2$	molar flow rate CO_2 at anode feed [kgmol/s]
ṅ$H2O$	molar flow rate H_2O at anode feed [kgmol/s]
ṅ$H2$	molar flow rate H_2 at anode feed [kgmol/s]
ṅ$CH4$	molar flow rate CH_4 at anode feed [kgmol/s]
ṅ$O2$	molar flow rate O_2 at anode feed [kgmol/s]
ṅ$N2$	molar flow rate N_2 at anode feed [kgmol/s]
nc	weighted average number of carbon atoms per hydrocarbon molecule in diesel feed
ne	number of electrons
nh	theoretical number of moles of hydrogen produced per mol of hydrocarbon
$ncells$	number of cells in SOFC stack
P	pressure [Pa]
Q	heat [kW]
r	rate of reaction [mol/m^3.s]
R	ideal gas constant [kJ/kmol.K]

Rp	pore radius
c	concentration [mol/m^3]
C	heat capacity [kJ/kg.K]
D	diffusion coefficient [m^2/s]
Eae	activation energy [J/mol]
F	faraday constant [C/mol]
H	enthalpy [kJ/kmol]
i	current density [A/m^2]
k	thermal conductivity [W/m.K]
K	equilibrium constant
LHV	lower heating value at anode feed [kJ/kg]
$LHVfuelin$	lower heating value fuel feed to SOFC system [kJ/kg]
$LHVfueltoref$	lower heating value fuel feed to reformer [kJ/kg]
$mfuelin$	mass flow rate fuel feed to SOFC system [kg/s]
$mfueltoref$	mass flow rate fuel feed to reformer [kg/s]
mCO	mass flow rate CO at anode feed [kg/s]
$mCO2$	mass flow rate CO_2 at anode feed [kg/s]

Chapter 1

Introduction

As evidenced by the development of the Kyoto Protocol in 1997 – which 190 countries have either signed or ratified [1] – and by the drafting of the Copenhagen Accord [(1)] in 2009, climate change is an issue of increasing importance. Both documents aim to fight climate change by mandating that countries reduce their anthropogenic greenhouse gas (GHG) emissions by power generators and automobiles, which contribute significantly to the phenomenon of global warming [2].

Awareness is growing that the world is experiencing a dual effect of reducing global energy supply while demand for those very supplies continues to increase. One of the more common responses to this has been increased usage of low grade fuel, which in turn has negative environmental effects. To solve this core issue it is imperative to extract as much energy per unit as possible with minimal environmental impact. Hence, modern day research and development studies on combustion have increasingly focused on the development of clean, compact, and efficient combustion systems.

CO_2 is a major product of hydrocarbon combustion that occurs in applications ranging from power generation to transportation. While efforts are being made to reduce CO_2 emissions, technologies are being developed to effectively prevent large quantities of CO_2 from being emitted into the atmosphere. Fuel cells generate electricity with low to zero emissions and provide not only environmental savings, but also productivity improvements: time, cost and manpower savings. No other energy generating technology offers the product range and combination of benefits that fuel cells can. The Solid Oxide Fuel Cell is a developing technology with significant potential benefit for power generation in automobiles as well as household energy needs. Unlike other fuel cells, the SOFC is capable of dealing with the mixtures of hydrocarbon fuel components. Overall thermal efficiencies are high; typically in the 45 to 50% range

[1] Which endorses the continuation of the Kyoto Protocol.

for conversion of the fuel bound energy to electricity on an LHV basis [5]. Also, the exhaust heat from the SOFC is at very high temperatures and may be used in a bottoming cycle or recovered for the generation of steam for cogeneration purposes which further increases the efficiency. It also reduces the release of pollutants such as SO_x and NO_x, and minimizing the release of unburnt fuel and carbon monoxide into the atmosphere, making SOFCs an environmentally viable option. The final result is the release of carbon dioxide to the atmosphere along with a large amount of water (steam) and nitrogen.

The SOFC presents a new and better way to produce electricity:

1. It can produce more energy per mole of fuel than a normal combustion engine.
2. Energy for system components, such as pumps and heat exchangers, is provided (partly as heat) by burning of excess fuel in the after burner, allowing the system to self-sustain.

The application of these SOFC systems in remote communities will provide further cost benefits. Increasing the efficiency of the system will result in less diesel burnt in the generator to produce same amount of energy. This will further reduce the cost of transportation of fuel to these remote locations.

1.1 Background

Solid Oxide Fuel Cells (SOFCs) are viable for generating electricity from hydrocarbon fuels, and integrate efficiently with reformers. The high operating temperatures (between 700°C – 1000°C) for these fuel cells promote rapid kinetics with non-precious metals. At the same time, however, this high temperature places stringent requirements on the materials. For this reason, the development of suitable low-cost materials and low-cost fabrication of ceramic structure has been a focus of much research. Research has yielded the correct materials for SOFCs to integrate well with large coal gasification plants which can produce high efficiency of 99% CO_2 capture, and low water consumption [4].

There are two major designs being developed by research centers at the moment – motivated by: i) how to seal the anode and cathode departments, ii) ease of manufacturing, and iii) minimizing losses due to electrical resistance. The two main designs, then, are tubular and planar. Operating between 900°C and 1000°C, tubular SOFCs have relatively high electrical resistance but are simple to seal [3]. Some tubular designs eliminate the need for seals altogether and allow for thermal expansion. Many of these units are operating now in the field with tens of thousands of hours of demonstrated operating time. Air is introduced inside of each tube while fuel flows over the outside of the cells. Oxygen ions migrate through the electrolyte to react with the fuel, and the flow of ions produces electricity.

Planar SOFCs are composed of flat, thin, ceramic plates. They operate at lower temperatures of 800°C or even less. Thanks to ultra-thin electrode / electrolyte sheets this form has low electrical resistance, allowing them to achieve high power density and efficiency [5]. Operating at lower temperatures also allows for the planar design to be composed of less exotic materials – lowering the cost of manufacturing. The anode, electrolyte, and cathode form thin, flat layers sintered together and then separated by bipolar plates. The planes could be rectangular, square, circular, or segmented in series [5].

With hundreds of stack tests having been run by Versa and Delphi and record-breaking electrochemical performance, the planar SOFC has come to the forefront as the high efficiency, low cost alternative [4].

1.1.1 Fuel Processor Configuration

Design of a fuel processing system is determined by the type of fuel cell used. Two distinctive system applications can be used to demonstrate the difference between a low temperature and a high temperature fuel cell [6].

For a SOFC system, the inlet feed has to be preheated and desulphurized .The feed is then mixed with air and steam. The adiabatic reformer is heated using anode-out gas as heat source. All higher hydrocarbons are reformed through steam reforming, thereby preventing formation of carbon in the reformer and anode

[6]. The fuel gas and air temperature is increased to approximately 650°C in the pre-heaters [7]. Air is used to cool the stack on the cathode side. Off gas is sent to the catalytic burner (or after burner) to produce heat for fuel pre-heating and steam generation during the initial (start-up) phase [7].

According to Shekhawat [8], fuel utilization should be set to 85%, with the fuel cell voltage set to be as 0.75V. Some other efficiencies given are shown below:

Air compressor = 72%,

Anode recycle blower/compressor = 55%,

DC/AC inverter =95%.

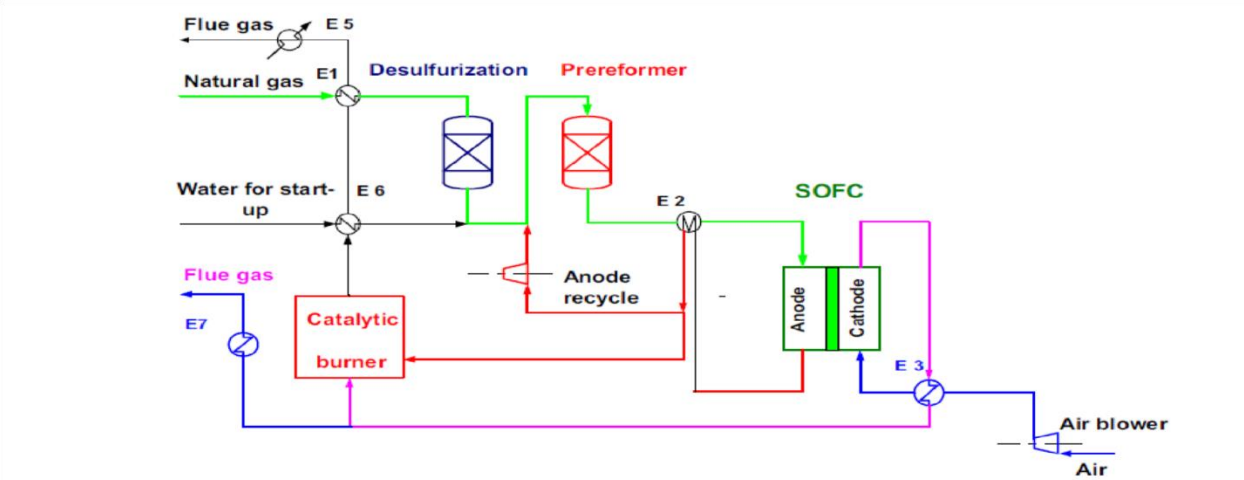

Figure 1: Basic layout of a 250-kWe SOFC-based CHP system; Taken from Fontell et al.. [6] and also given in Shekhawat [8]

1.2 Present Developments and Barriers in SOFC Systems Application

Cost reductions over the years in the development of industrial SOFC systems have been encouraging. The Department of Energy (DOE) has estimated that for a 5 kW planar SOFC and Gas-Turbine hybrid system, a cost of $400/kW can be achieved at reasonable manufacturing volumes [9]. The DOE initiated

the Solid State Energy Conversion Alliance in 2001 and aimed to reduce the cost to less than $400/kW by 2010 [9]. According to a research conducted by Rolls Royce, SOFC costs of $300/kW are already possible for large gas-turbine based hybrid systems. The majority of estimates, however, are in the range $700/kW to $1300/kW [10]. Several companies in Europe are already offering stack modules and complete units at a pre-competitive level for demonstration projects in niche markets. The use of biogas is also a major option in Europe as a renewable energy source. Biogas is receiving much attention as it is a source of GHG-neutral methane.

There are more than 80 companies in Canada as listed by Industry Canada, whose primary focus is the development of fuel cells and its systems [11]. An SOFC Canada (SOFCC)-NSERC Strategic Network [12] has also been established and represents and facilitates collaboration between 21 Canadian research groups from both university and governmentally supported industry. SOFCC is focusing primarily in Northern Canada, where an infrastructure for the transportation of diesel fuel exists and electricity costs on a per kWh basis are competitive with SOFC technology [12].

There are no moving parts in a SOFC system and therefore there is less vibration and noise than a combustion engine. The operating temperature of a SOFC provides heat for reforming of the fuel for the anode. This results in improved thermal integration through regenerative heat recovery from the SOFC stack [13]. SOFCs also have a high fuel to electricity conversion between 45% and 65%. The total SOFC system efficiency including recovery of high-quality waste heat can increase to 85% [13]. SOFCs have been constantly in the development period among all fuel cells, with the first fuel cell developed in 1950's. New materials development for SOFCs to drive down costs, material durability and the lifetime of the stack has been an important technological and research driver. Some of the focal points have been in the development of new sulphur and coke tolerant anodes, metal-supported cells for improved fabrication costs and durability as well as robust interconnects and seals [12].

Although the technology for SOFCs has long been promising, one major problem yet to be overcome is the limited lifetime of the SOFC stack. Over time, the wear and tear of materials at high operational temperatures results in thermal stresses. These can eventually lead to mechanical failure of components at their interfaces and limit the lifetime of the stack to approximately five years at full-load with reference to 2005 technology [10]. The future direction is aimed towards fabrication of low temperature SOFCs below 650°C.

1.2.1 Government Regulations

In April 2007 the Government of Canada announced Turning the Corner: An Action Plan to Reduce Greenhouse Gases and Air Pollution. This established a commitment to reduce GHG emissions to 20% below 2006 levels by 2020, and to reduce them a further 60-70% by 2050. The enactment of the program was postponed to provide the opportunity to fine-tune the approaches to tackle climate-change. In 2007, the Government of Canada drafted the Regulatory Framework for Air Emissions, which provides a great source of reference for companies in preparing for pending federal regulation. The federal government built upon this framework in 2008 with the release of the Regulatory Framework for Reducing Industrial Greenhouse Gases.

The regulations will mandate reductions in emissions of greenhouse gases and air pollutants from two industrial sectors: power generation and oil and gas sector. The federal government will require facilities in those sectors to report emissions and other relevant data under a notice issued under section 71 of the Canadian Environmental Protection Act, 1999.

Fuel cell emission streams usually contain only trace amounts of CO, NO_x, SO_x, unconsumed hydrocarbon and particulate matter. From a human health standpoint, these compounds are more harmful

than CO_2 and can be linked to acid rains and global warming. The cost of reduction for these pollutants may be best described by the added equipment to comply with regulatory guidelines.

Diesel Generators, usually run on JP-8 or gas oil with high carbon content[20]. The output gas from these systems, usually released directly into the atmosphere, is environmentally unfriendly with its high content of unconsumed hydrocarbon, carbon dioxide and carbon monoxide that are all classified as the greenhouse gases.

1.2.2 Environmental Impact:

With low emissions of pollutants such as nitrogen oxides (NO_x), sulfur oxides (SO_x), as well as dramatically lower emissions of carbon dioxide (CO_2), SOFCs qualify under several environmental certifications established by the government. Some of these include the "Leadership in Energy and Environmental Design" (LEED) program and the "Renewable Energy Standards" (RES) program [14].

1.3 Diesel Generators vs. Diesel-fueled SOFC systems

Many rural areas in Northern Canada have diesel generators for back-up power and most of the farms are run on diesel power [12]. This has proved expensive over the years as the overall efficiency of diesel engines is found to be 20-25% and the price of diesel has been on the rise [20]. The following graph shows the change of diesel price during the past four years.

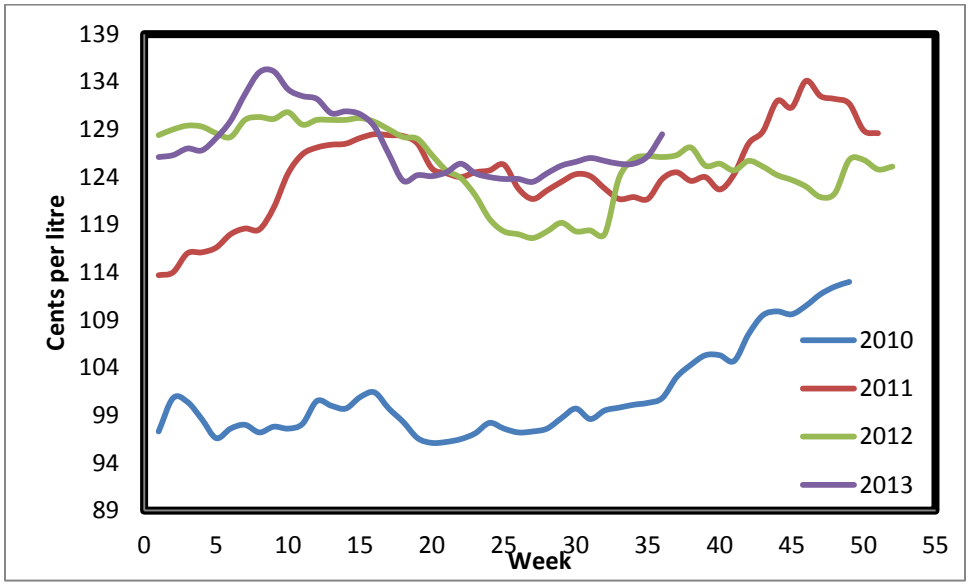

Figure 2: Diesel Price over the past 4 years (Data taken from Natural Resources Canada Website [15])

Figure 2 shows the normalized price of diesel over the past 4 years. It can be seen that there has been major increase in the diesel price and this directly affects the energy production cost for farmers.

With diesel engines producing a high amount of GHG emissions into the atmosphere, many environmental organizations have been working hard to reduce emissions by supporting the commercialization of renewable low emission engines. The emission of GHG negatively affects crops and cattle around the farm. This has urged many farmers to look at different options for electricity and energy. The maintenance cost of SOFC power systems is very low and they have high efficiencies, hence more energy is produced, enabling rural farmers to operate off-grid.

Alternate technologies such as wind and solar power also provide clean energy and can rival the entry of fuel cells in the market. However these technologies are not very efficient and the power produced is very low [17]. Since, wind and solar power is still not common in the market, it is a very expensive exercise to purchase and install the solar panels and wind turbines, to match the power produced by a combustion engine or a similar rated fuel cell system.

To counter the low efficiency and scarcity of diesel fuels, many companies, such as G.E., are working towards producing gas engines that are more efficient and can run on ethanol. These can be a substitute to SOFC power systems in the residential markets, if mass production of these engines occurs.

To further the analysis of production of SOFC power systems for farms and rural areas, Gartner's quadrant analysis is conducted. Although, this is a new market, with very few entrants, there are some major companies in the commercial market that could jump into residential application if they find other companies making an entry into that market. The R&D departments of these companies have been working on developing different process designs for different markets for fuel cells.

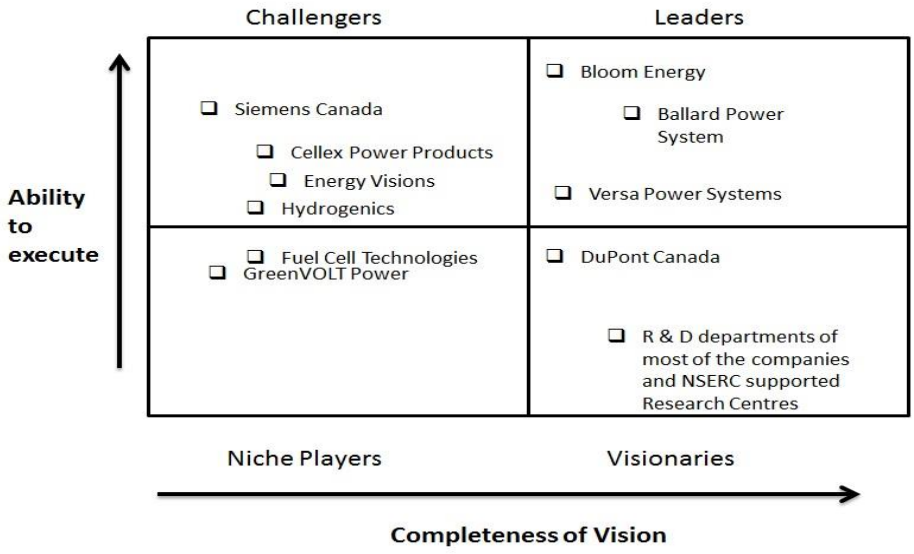

Figure 3: Gartner's Quadrant Analysis for SOFC power systems

The low emission and noise characteristics of fuel cells make them an ideal replacement to diesel generators for farms and rural areas. With the potential end user mostly farmers, it is very important for them that the overall cost to run their farms gets lower. Novel SOFC systems, that use biomass and organic plant waste as primary fuel, may obviate the expense of 'purchasing' a fuel source, as well reduce GHG emissions. This cost benefit may accrue over the years, making the switch to a SOFC system more financially plausible.

An analysis by Fuel Cell Today indicates that approximately 24,000 fuel cell units shipped in 2009, this represents an increase of 41% compared to 2008 [19]. Early market applications include fuel cell power for materials handling equipment, backup power, telecommunication towers, data servers, and primary or backup power for retail sites and commercial buildings [19].

1.4 Scope:

The scientific aim of the present work was to gain insight into the design and optimization of a 1kW diesel-powered SOFC system that could be implemented in rural areas of Canada. To achieve the goal, following sub-theme targets were identified:

1. Develop a steady-state process simulation of a 1kW diesel-fuelled SOFC system.
2. Design and characterize a steady –state model for a ceramic tail-gas burner.

The simulation software package, VMGSim^{TM} was used to design the 1kW diesel-fuelled SOFC system. The software was also used to estimate the efficiency of the system. A preprogrammed fuel cell unit operation (beta testing package made recently available) was used to evaluate the performance of the fuel cell. Such a system could potentially replace combustion engines as a source of power in rural areas. In order for the system to function as a viable alternative, the SOFC system would need to be able to generate 1kW power that could be turned into electricity.

COMSOL^{TM} was used to design and characterize the model of a ceramic tail-gas burner of this 1kW SOFC system. Thermodynamic, transport, and flow analysis for the tail-gas burner were conducted during the research. The model was validated using the experimental data, which was collected at the NRCC-IFCI and provided by Adam Tuck. A pre-mixed fuel-air stream analysis was conducted and compared to the base case performance.

1.5 Thesis Outline:

The thesis is subdivided into six chapters. Chapter 1 gives an overview of the many aspects of fuel cell systems followed by a discussion of development and barriers in the commercial application of SOFCs as well as a comparative overview as why diesel fuelled SOFC systems are preferable to diesel generators. Chapter 2 reviews some of the existing literature on diesel-powered SOFC systems and tail-gas burners. Chapter 3 discusses the system design of a 1kW SOFC diesel fuelled system, with a new fuel cell unit operation used to define the fuel cell in VMGSim™. Chapter 4 analyzes the design of a tail-gas burner model in COMSOL™. Chapter 5 summarizes the principal findings and provides recommendations for the system design and tail-gas burner model.

1.6 Works Cited

[1] United Nations Framework Convention on Climate Change. (2009, December 3). Status of Ratification. Retrieved March 28, 2012, from United Nations Framework Convention on Climate Change website: http://unfccc.int/files/kyoto_protocol/status_of_ratification/application/pdf/kp_ratification_20091203.pdf

[2] United Nations Framework Convention on Climate Change. (n.d.). The Greenhouse Effect and the Carbon Cycle. Retrieved March 28, 2010, from United Nations Framework Convention on Climate Change website: http://unfccc.int/essential_background/feeling_the_heat/items/2903.php

[3] Energy, U. D. (2004). Fuel Cell Handbook 7th Edition. Morgantown, WV.

[4] Surdoval, W. (2009). U.S. DOE's stationary fuel cell progream: Energy production in carbon challenged world. Palm Springs, CA: Department of Energy.

[5] Shekhawat, D. (2011). Introduction to Fuel Processing. Amsterdam: Elisvere.

[6] Fontell E, K. T. (2004). Conceptual study of a 250kW planar SOFC system for CHP application. Power Sources, 49-56.

[7] Rostrup-Nielsen JR, C. L. (2011). Concepts in Syngas Preparation. London: Imperial College.

[8] Rostrup-Nielsen J.R. (2011). Steam Reforming in Fuel Cells. In D. Shekhawat, Fuel Cells: Technologies for Fuel Processing (pp. 63-65). Amsterdam.

[9] N.R. Council. (2004). The hydrogen economy: operation, costs, barriers and R&D needs. National Academy Press.

[10] Hawkes, A. (2007). Cost-effective operating strategy for residential micro-combined heat and power. Journal of Power Sources, 74-81.

[11] Industry Canada. (n.d.). Retrieved July 4th, 2013, from Hydrogen and Fuel Cells; : http://www.ic.gc.ca/eic/site/hfc-hpc.nsf/eng/home

[12] Retrieved June 2012, from SOFC Canada: http://www.sofccanada.com/Documents/SOFC%20XII%20Network%20Talk.pdf

[13] Shekhawat, D. (2011). Introduction for Fuel Processing. In Fuel Cells: Technology for Fuel Processing (pp. 3-5). Amsderdam: Elisever

[14] EG&G Technical Services. (2002). Fuel Cell Handbook 6.

[15] Natural Resources Canada. (n.d.). Retrieved July 20, 2013, from Energy Resources: http://www2.nrcan.gc.ca/eneene/sources/pripri/prices_byyear_e.cfm?ProductID=5

[16] Hoogers, G. (Ed.). (2003). Fuel Cell Technology Handbook. CRC Press.

[17]Earth 911. (2007, October http://earth911.com/news/2007/10/15/pros-and-cons-of-solar-power/). Pros and Cons of Solar power.

[18] SOFC network. (n.d.). Retrieved April 2011, from SOFC network: http://www.sofccanada.com/primer.html

[19] Gangi, S. C. (2010). The Business Case of Fuel Cells. Fuel Cells 2000.

[20] Speight J, (2011). The Biofuels Handbook, RSC Publishing.

Chapter 2

Literature Review

This chapter reviews the information available in published articles and papers concerning i) the analysis of small scale SOFC systems, and ii) the modelling techniques and optimization of ceramic porous tail-gas burners. Section 2.1 provides a background overview of fuel cell systems. Section 2.2 discusses at different system designs, performance phenomena and the efficiency of small-scale SOFC systems. In section 2.3 the main focus is on the design and characterization of ceramics porous media burners. Pre-mixed and non-mixed feds are also briefly reviewed in this chapter.

2.1 Overview of Fuel Cell Systems

Most fuel cell systems require certain components to ensure efficient and safe operation. The stack and these components together form the fuel cell system. Most of these fuel cell systems require similar components for certain key operations, yet set up according to individual stack designs and fuel used [1].

The fuel is first processed prior to entering the fuel cell stack. Steps of fuel processing includes desulphurization, reforming of inlet fuel using steam, to produce H_2 rich mixture, which is then fed to anode of the fuel cell stack. In the fuel cell stack, the fuel consumed from the electrochemical reaction generates a power output based on the stack current and voltage. In the case of high-temperature fuel cells, however, direct oxidation of CH_4 and CO is also possible at the stack anode. This reduces fuel processing requirements upstream of the stack. In addition, the system also requires air, fuel and water management using compressors, blowers, pumps and air filters. A process control scheme is also required in order to maintain the desired operating conditions of the system. During fuel processor's analysis, the stack temperature and the inlet flow to the fuel cell system are some of the variables that need to be

controlled for required output. Precise control of the process variables is critical to the viability and robustness of fuel cell systems [2]

2.1.1 Fuel Processor

Most fuel cells rely largely on hydrogen-rich reformate and water in order to operate. Unfortunately, hydrogen gas is not easily available as the infrastructure (unlike that for petroleum or diesel) simply does not exist. Fuel processors, then, are designed to extract the necessary inputs from more conventionally available hydrocarbon fuels. These include but are not limited to: methane, methanol, ethanol, propane, gasoline, jet fuels, diesel, and biodiesel. Since each fuel cell requires a specific input, though, fuel processors must be custom built to provide this.

A standard fuel processor converts a liquid fuel into a CO-free gas stream containing only H_2 and O_2. Often water is also added during the process to achieve the two objectives of minimizing catalyst deactivation, and increasing the yield of H_2 [1]. Depending on the type of the fuel cell, the process normally includes: conversion of the fuel into syngas, a water gas shift (WGS), and preferential oxidation of CO.

2.1.2 Fuel Flexibility:

As adoption of fuel cells increases across the globe, it will be essential to see the creation of a network of hydrogen rich gas streams. This will require the fuel cell processors to generate some relatively uniform hydrogen-rich gas from relatively diverse collection of fuels available in different locations. Some of these include: natural gas, ethanol, gasoline, and diesel. These fuels all have their own unique mix of methane compounds, aromatics, and contaminants (such as sulphur) that must be removed. The post-reformer treatments required for this could include sulphur removal, and water gas shifts [1].

Despite their logistical ease these fuels are highly complex and variable mixtures of hundreds of hydrocarbon compounds containing olefins, alkanes, napthenes, and aromatics [1]. These fuels also have pyrolytic and carbon-forming tendencies which can lead to carbon deposition. Also, the differing boiling points of these components can make mixing in fuel processors and fuel vaporization difficult.

For the use of these fuels, fuel processors need to be designed to generate a relatively uniform hydrogen-rich gas stream from the wide range of fuels, with emissions remaining under the regulatory requirements for greenhouse gas emission.

2.1.3 Diesel Fuel:

Diesel fuel characteristics fall into various categories: volatility, ignition, quality, viscosity, gravity, stability. Much like gasoline, diesel fuel additives are also available to make it more commercial and feasible for combustion engines [3]. Also like other fuels, diesel fuel has difficulty starting below a certain temperature in cold weather. As SOFCs operate at high temperatures, this problem can be averted by utilizing diesel as an inlet fuel for fuel cells. Furthermore, the SOFC ensure that the greenhouse gases emitted by burning diesel fuel fall under the proposed regulations of the government. The allowable sulphur content for low sulphur kerosene and diesel (15ppm) are much lower now than they were in the past (500ppm) [3]. This new regulation not only mandates a reduction in the emission of sulphur compounds (which cause acid rain), but also allows the installation of advanced emission control systems, which would otherwise be poisoned by these compounds. In the past diesel was distilled straight from crude oil, however, as demand has grown diesel goes through various cracking processes to produce distillates and increase the volume available in the marketplace. Much care is taken to ensure that the cracked stock is selected and mixed in such a manner that all regulatory expectations and all legal specifications are met.

Since diesel contains different types of contaminants, it requires different types of catalysts and post reformer treatment processes, such as desulphurization and water gas shift reaction in the fuel processor system. Diesel is relatively difficult to reform, therefore, both catalyst and reactor design are essential to the fuel processor.

2.1.4 Reforming Modes:

The three main methods of catalytic reforming are: partial oxidation (POX), stream reforming (SR), and oxidative stream reforming or auto-thermal reforming (OSR) [1]. Hydrogen-rich synthesis gases are the end result of all three processes – this is done through the oxidation of some hydrocarbon fuel. The actual chemical reactions are shown below [1]:

$$\text{POX: } C_nH_m + (n/2)\ O_2 \rightarrow nCO + (m/2)\ H_2 \quad \text{(Equation 1)}$$

$$\text{SR: } C_nH_m + nH_2O \rightarrow nCO + (n + m/2)\ H_2 \quad \text{(Equation 2)}$$

$$\text{OSR: } C_nH_m + H_2O + O_2 \rightarrow CO + H_2 \quad \text{(Equation 3)}$$

The standard fuel cell processor is either catalytic or non-catalytic; this is an important distinction and has a large impact on overall efficiency and the operating characteristics of the fuel cell system.

Catalytic fuel cell processors normally have temperatures ranging from 600°C to 1000°C [4]. Non-catalytic systems are more costly, require higher temperatures and more expensive materials. Due to these reasons, non-catalytic systems are not widely used.

2.1.5 Steam Reforming (SR):

Steam reforming is a normal process in the petrochemical industry in their refineries [5]. A major part of the hydrogen consumed in refineries has always been produced as a by-product of other refinery processes like catalytic reforming. Given the increasing demand required for the deep desulphurization of

fuels in the new regulatory environment, the need for increased hydrogen production is growing rapidly [6]. To meet this need there has been an increase in the installation of steam reforming-based hydrogen plants.

Steam and methane have a highly endothermic reaction driven by the entropy resulting from the formation of new particles. Methane conversion is favored by high temperature, low pressure, and a high steam to carbon ratio.

2.1.6 Auto-thermal Reforming or Oxidative Steam Reforming (OSR):

OSR can be considered a combination of partial oxidation and steam reforming. Feeding air and steam together utilizes the heat generated from exothermic oxidation of the fuel to promote the endothermic steam-reforming reactions. In the reformer, the heat from the oxidation reactions thermally balances the endothermic steam reforming reactions, rendering the overall reaction thermo neutral. Although, OSR is considered thermo-neutral theoretically, in reality there are heat losses from the system. This can be countered by running the overall system at higher oxygen to carbon ratio. The oxygen to carbon ratio usually depends on the feed composition and the structure of the carbon in the fuel. Optimum operating conditions for OSR are given below [7]:

O/C ratio: 0.7- 1.0

S/C ratio: 1.5 – 2.0

Temperature: 700 – 800°C

2.1.7 Fuel Processor design:

Oxidative steam reforming of diesel fuel is less energy intensive compared to SR due to the catalytic oxidation of the fuel which enables further energy supply to the reformer. There is also a lesser risk of

carbon formation in comparison to SR and POX due to the coexistence of steam in the feed. Studies regarding diesel reforming show that the inlet ratios of S/C and O/C should be between the range of 1.5-3.0 and 1.0-2 [8]. However, results for ratios outside these ranges have also been reported for different feed compositions and inlet fuel [9]. Reaction temperatures are in the range of 800 - 1100 K [8]. The sequential occurrence of POX and SR reactions has been generally agreed upon as the mechanism of OSR and has been further supported by the observations of hot-spots along the reformer [9]. Moon et al. [10] observed that decreasing the O/C ratio reduced H_2 and CO yields, while increasing CO_2 yield, indicating POX stoichiometry. To ensure careful design of the mixer and heater, the reformer should be chosen with good heat transfer characteristics and its design must be robust enough that temperature spikes should not affect the overall system.

2.1.8 Hydrogen production:

With many commercially available fuels being used for power production by fuel cells system, hydrogen production is required by fuel cell systems for optimum performance. Hydrogen production in plants typically occurs at high supply pressures. High S/C ratios are thermodynamically favoured in a diesel fuelled SOFC systems. When low S/C ratios are used, it limits mass flow, thereby producing less heated gas in the reformer. With a low S/C ratio, more fuel remains unconverted from the reformer, and is ultimately converted through internal reforming in the fuel cell. The energy is then recovered by a tail-gas burner for burning up to 99.999% H_2 into energy [1]. The resulting off-gas from the burner provides heat to the reformer.

A higher pre-heat temperature with low S/C ratio may help in achieving a higher hydrogen production. For optimum results, S/C ratio as well as temperature of the feed should be given chosen from ranges given above.

2.1.9 Carbon formation:

Carbon forms in different ways in the SOFC systems. Nickel crystal is formed as fibers from carbon monoxide, methane, and other higher hydrocarbons. This growth can be stunted, however, by sulphur poisoning and is slower on noble metals [11]. The rate of carbon formation is far less on noble metals than on nickel [12]; hence noble metals as catalysts should be used. In the presence of higher hydrocarbons, thermodynamics and steam to carbon ratio (S/C) also helps in estimating the risk of carbon formation [13]. Type of inlet fuel, catalyst and temperature of the reformer can be altered to decrease the carbon formation.

2.1.10 Diesel Desulphurization:

The low sulphur content of regulated fuels such as jet fuel and diesel, along with their wide availability and high energy density make them ideal choices for the inlet fuel for small fuel processor systems. The sulphur concentration of diesel is currently being regulated to 15ppmw sulphur, while sulphur in jet fuels is, at times, allowed to be as high as 3000 ppmw per requirements [14].

The boiling point ranges for the stated gases are as follow: gasoline: 38-204°C, jet fuel (JP-8):175-300°C, and diesel: 149-371°C [14]. The presence of diesel in the inlet feed also implies that liquid phase desulphurization would be a more feasible option as it allows adsorption to take place at lower temperatures. Given heavier petroleum products such as jet fuels and diesel, oxidation-assisted adsorption may also be an option although such a method has not been extensively researched.

The choice of sorbent to use for the desulphurization of the inlet fuel by adsorption however, has been a topic of extensive discussion. Babich and Mouljin [15] have reviewed the research and development of common sulphur adsorbents for fuels, such as diesel. During this time, activated carbon, zeolite 5A,

zeolite 13x, silica alumina, and alumina were tested as possible sorbents [14]. Most of these adsorbents carry out separation based on the polarity. .

Based on the review, in Shekhawat et al. [14], gas phase and liquid phase desulphurization can be done either downstream or upstream of an oxidative steam reformer, from liquid fuels such as diesel. In OSR, the fuel is mixed with air and steam, which caused volumetric reduction of the sulphur concentration in the stream to the reformer. For small and compact fuel processors, single step liquid desulphurization can be used.

2.2 SOFC Systems:

Lawrence et al. [16] discusses an Auxiliary Power Unit (APU) of a SOFC, which is fuelled by diesel and thermally self-sustaining. Diesel was selected since it is the most readily available and practical inlet fuel and is commonly used for applications in the truck and residential power markets [17]. This APU SOFC system produced 1kW of electrical power and did not use any external water supply, thereby reducing both system costs and potential failure modes. The unit was built in collaboration with H.C. Strack GmbH and Fraunhoker IKTS with three core features: (i) a dry catalytic partial oxidation (CPOX) diesel reformer, ii) 30 cells SOFC stack with an open cathode, and iii) a porous-media afterburner [18].

The paper presented a number of pertinent findings which proved relevant to this thesis related research. The APU system demonstrated thermal self-sustainability and operation without an external supply of water. Second, the system is able to start without the use of any heating elements, purge gas, or tolerance systems to transients, and can have an emergency shut-down. This APU was also operated for over 4 hours at a stretch without and discernible degradation to the stack, thereby demonstrating that the “dry” CPOX reformate is acceptable to the stack. Finally it was found that a top-down system design process

could be used to design a similar system. This process resulted in a simple system design with the primary components of an SOFC system a stack, a reformer, and an afterburner all integrated into a single hotbox.

This paper also reports that a thermally self-sustaining operation is possible with stacks of only 10 or 30 cells, and the system does respond stably to interruptions such as step changes in stack current. Second, the temperature within the hotbox can be controlled by simply altering the flow of diesel entering the system (reformer power) and toggling this amount. Third, even finer (but slower) control can be obtained by altering the cathode air flow rate. It was also important to understand that the redox tolerant stack allows significant simplification of both the start-up and shut down process. Finally, it is determined that the open cathode and low pressure drop within all system components produced a total system pressure drop of less than 30 mbar.

There are three major limitations of the methodology undertaken in this paper. First, it does not look at the effect of varying of the O/C ratio or the S/C ratio. Second, it limits findings to only 10 and 30 cell stacks, not giving us an understanding of the broader spectrum. Finally, it does not discuss much about how varying temperatures in the hotbox (done by changing the rate of diesel flow as noted earlier) effects the reformer and porous media afterburner.

In his paper, Roychoudary [19] describes the design and sizing of a prototype for a 5kW fuel-processor powering a solid oxide fuel cell (SOFC) stack. The system consists of a small, modular catalytic Microlith auto-thermal (ATR) reactor with the versatility of operating on diesel, Jet-A of JP-8 fuels [20]. The substrates and catalyst technology utilized in the reforming reactor is a more recent and patented technology.

The paper had a number of interesting findings, which have been overviewed. First, the reactor demonstrated the capability of efficiently reforming liquid and gaseous hydrocarbon fuels at exceptionally high power densities. The transition to steady operating conditions took approximately 1 minute. More air

is then added and the complete conversion into hydrogen is achieved. Unlike in the previous paper, different catalysts were tested for durability with the S/C ratio between 1.1 and 1.7 and the O/C ratio between 0.96 and 1.35. During this process the inlet temperatures were kept between a range of 150 and 400°C. It was found that the fuel conversion in the reactor was between 63% and 84%, when the inlet temperature was set as 150°C, while the overall conversion jumped to between 78% and 94% when the inlet temperature was 400°C. The variability at each temperature was driven by changing S/C and O/C ratios. This paper also discussed the integration of steam generators, desulphurizer, pumps, blowers, and controls with the fuel cell processor. Lower S/C ratios generally mean that the system needs less water, which can be recovered from the SOFC exhausts. Fuel preparation for the system is also discussed briefly, while the power density was found to be approximately 1kg/kW.

This paper also explains that the system was developed via ASPEN Engineering Suite process simulation software and was analyzed with reference to system balance requirements. Second, the integration of the ATR reactor with a SOFC system will result in a slower stack heat-up rate and became a design consideration. Finally, it was recognized that Aspen is similar to UNISim^{TM} and VMGSim^{TM} simulation softwares (which is used in this thesis's study), so this study can be used to learn how the fuel processor is setup in these softwares.

In this study two major limitations were apparent. First, since the fuel processor has not been integrated with fuel cell, aspects of thermal integration with the stack have not been specifically addressed. Second, a disproportionate amount of the focus is on discussing the Microlith auto-thermal reactor, while there is almost none on the power generation and factors affecting the system.

Lisbona et al. [21] developed a model for a 1kW solid oxide fuel cell (SOFC) for the purposes of decentralized electricity production and then studied. The proposed system operated on natural gas and consists of a planar anode supported fuel cell section and supports by components such as: gases suppliers, a fuel processor, a heat management system, an after-burner, and a heat conditioning system.

Microsoft Excel, Visual Fortran, and Aspen Plus™ were the three softwares employed to design the system. This process model enabled the prediction of the system as closely as possible by using mass and energy balances, reaction kinetics, and phase and chemical equilibrium calculations [21]. An in-house code for SOFC stack black-box model in FORTRAN was developed and linked to the main commercial simulator as a user model subroutine. The components of the balance of plant have been implemented using Aspen Plus™ modules. Pressure losses of 5% are assumed at every stage of the system. In this system, natural gas is passed through a simple desulphurizer module, which is made out of an activated carbon bed. After the gas passes through the SOFC stack, anode-off gas is fed to the afterburner. The afterburner itself is kept adiabatic and the anode-off gas is burnt with the non-recycled part of the oxidant flow [1]. The reactions carried out are [1]:

$$H2 + 1/2O_2 \rightarrow H_2O \quad \text{(Equation 4)}$$

$$CO + 1/2O_2 \rightarrow CO_2 \quad \text{(Equation 5)}$$

It was assumed that the hydrogen reaction consumes 95% of the hydrogen in the anode-off gas. The electrical and thermal efficiency of the system for non-reference conditions were evaluated. The effect of the deviation from the reference conditions of fuel utilization, gas temperature, spring in fuel cell stack, anode off-gas recirculation rate, air inlet temperature and external pre-reforming reaction were also analyzed in this paper. The results of this process design show that electrical efficiency of 45-51% can be achieved in a wide range of operating conditions. Among the investigated parameters, the degree of pre-reforming is the only one, which has always had a positive effect on the electrical efficiency of the system. If the degree of pre-reforming is enhanced, the power production directly increases; much of this is because of the higher H_2 content in the inlet anodic gas. For fuel utilization of less than 60% it was found that the improvement in electrical efficiency is not valuable, given the significant reduction in thermal efficiency, which almost outweighs the benefits. Heat for the system is required at a very high temperature and the combustion of the SOFC exhaust in the after-burner could not be sufficient to achieve these temperatures, especially when fuel utilization rates are high. The electrical efficiency is high when

one varies anodic recirculation and fuel utilization. . This paper also shows that the value of electrical efficiency is maximized when the value of fuel utilization shits from 0.75 to 0.95 and one increases the degree or pre-reforming from 20% to 60% while decreasing anodic recirculation from 75% to 40%. The study also reveals that in general the electrical and thermal efficiency follow opposite trends, thus an increase of electricity determines a reduction of exported heat, and vice versa.

There were three main findings from this paper. First, the dependence of electrical efficiency on the anodic recirculation ratio, pre-reforming degree and the value of fuel inlet utilization were relevant. Second, this study proved a powerful tool for evaluation the SOFC system performance under a wide range of operational conditions and paves the way to defining control strategies in order to maintain high system efficiency under part-load operational conditions. Finally, the global efficiency follows the trends of thermal efficiency, as it is much more sensitive than electrical (or other efficiencies) to the variation of operating parameters.

Much like all the others, this paper also had a few limitations, which needed to be taken into account. First, this paper speaks about further study using a fuel-cell unit model in this system design, but the use of a fuel cell unit model can change the approach. Second, the study also did not test the effect of concentration of gases in the anode off-gases to the afterburner, or how the change of fuel inlet type would affect the system. A study with different flow configurations will be required to truly understand the actual thermal efficiency in the system. Finally, the recirculation of exhaust gases from the cathode must be studied and designed in order to optimize heat utilization given the temperature spring of the flows in every heat exchanger.

Similar to Lisbona's research, Zink et al. [22] developed a black-box SOFC model to assess an integrated system for district heating and cooling applications. The fuel cell model consists of heat and mass macroscopic balances, simplifying the electrochemical model through the definition of empirical input parameters such as fuel utilization.

Costamagna et al. [23] developed a 0D model of a SOFC/micro gas turbine (MGT) hybrid system to analyze a hybrid system under variable fuel cell and operating conditions. The fuel cell is modeled through macroscopic equations that express the balance between inlet and outlet conditions. These simplified approaches were used in order to save computational time while maintaining an acceptable accuracy in the overall plant performances assessment. Zink and Costamagna's research were discussed in length in Lisbona's paper as the two studies had similar output results and were used to validate Lisbona's research.

Yi et al. [24] examines the fuel flexibility of an integrated 25kW SOFC-reformer system at the National Fuel Cell Research Center in the University of California [25]. A total of four different types of fuel and compositions were investigated. These were: i) pipeline natural gas, ii) diesel reformate, iii) biogas, and iv) coal-derived syngas. A tubular design configuration of Siemens Westinghouse single cell per tube was used in the fuel cell stack [26]. The system was validated using the Advanced Power Systems Analysis Tools developed at the University of California [25]. Desulphurized fuel enters the bottom of the stack, and an ejector is used to create a particle vacuum to pull spent fuel from the anode side of the system. The reformed fuel is then distributed to the outer surface of the tubes. Cathode air is pre-heated using the system exhaust and then sent to the inner surface of the fuel cell tubes using air feed tubes from the top of the stack. Oxygen anions formed from the oxygen in the air, flow up inside the fuel cell tubes. These anions travel through the electrolyte and react with the oxidized fuel on the outside of the tubes. The Anode off-gas is then recirculated and burnt using the depleted air from cathode, in the combustion zone of the SOFC generator. An APSAT model was designed for the analysis of this 25kW system, and the fuel utilization was set to a constant value of 82%.

It was found that the difference in exhaust temperatures from the SOFC system when using biogas was only 7°C higher than that of natural gas. When diesel was used as the inlet fuel to the system, the exhaust temperature was only 21 degrees higher than that of natural gas. With coal syngas, the exhaust

temperature was found to be 153 degrees higher than natural gas. It was also found that coal gas yielded the lower system efficiency of 25.6% as compared to the other fuel sources. Natural gas, diesel and biogas yielded system efficiencies of 37.2%, 35.8%, and 36.1% respectively. It was stated in the paper that higher system efficiencies can be achieved by using gas turbines and producing useful work from recoverable heat in the exhaust. With the APSAT model, the error percentage in the observed and modelled value, for system efficiency is 2.5%. The error between the DC power values is 1.7%. Fuel compression was ignored in the model as pipeline natural gas is at a sufficient pressure and the syngases are assumed to be compressed prior to being delivered into the system. The anode off-gas recirculation ratio was varied with different fuel compositions in order to avoid the carbon formations while not considerably affecting system efficiency.

This paper discusses a few useful findings. First, the APSAT software can model the performance of the 25kW SOFC system and shows considerable capability to design systems that are similar to this. Second, the simulation results show that design conditions can be identified that allow the SOFC system to run on diesel reformate and yet produce performance similar to the performance of a natural gas SOFC system. The difference in the temperatures while using different fuels can be attributed to lower CH_4 content in those fuels. The significant increase in exhaust temperatures when using coal syngas is due to no CH_4 content and a high CO content, thereby promoting an exothermic Water-Gas Shift (WGS) reaction. For coal syngas higher system efficiencies can be achieved if the SOFC is coupled with a gas turbine or other generator that limits the exhaust heat loss. A proper design of the anode off-gas recirculation ratio could improve system efficiency further as well are reducing carbon deposition.

There were two major limitations identified in this study. First, the study does not use a ceramic afterburner after the SOFC stack to recover heat from the anode off-gas. Second, it did not test for the effects of a varying S/C ratio on the exhaust temperature using different fuel types.

Lastly, Dhingra et al. [27] paper is reviewed to understand the effect of varying certain process and operating variables on performance metrics. At the outset it must be stated that it is the opinion of the author that this study is an improvement of all studies reviewed prior to this when it comes to looking at residential SOFC system using diesel as a fuel source. This is perhaps because this paper is closest to the study that is being conducted in this thesis and therefore the most pertinent.

In this paper, a simulation of a 1kW diesel-fuelled SOFC system was developed and a sensitivity analysis was carried out to investigate the influence of important design variables on the system performance. Three objected variables are chosen in this paper to characterize the performance of the system: net system efficiency, gross stack efficiency, and exhaust temperature. The proposed system, operated on diesel reformate, consists of a planar anode supported fuel cell stack and components such as: blowers, a desulphurizer, pumps, a heat exchanger system, reformers, and an adiabatic afterburner. The system is modelled in process simulation software, VMGSim^{TM} with Microsoft Excel used to design the fuel cell stack and the reactions occurring inside of it. The afterburner exhaust is used as the primary heating utility for the system and negligible pressure dropped is assume throughout the system. The desulphurizer is a simple liquid adsorption separator. The auto-thermal reformer and the afterburner are used to be adiabatic and thermo-neutral operation for the auto-thermal reformer.

The gross stack efficiency and net system efficiency were observed to be most sensitive to the fuel (reformate) and air utilization on the stack. The system exhaust temperature, on the other hand, was most sensitive to the S/C ratio, because higher temperature vaporization was required at higher ratios to generate steam. It was found that, at lower fuel utilizations, higher air utilization factors were not desirable. A maximum net system efficiency and gross stack efficiency of 45% and 47%, respectively, were observed at $U_f = 0.9$, $U_a = 0.5$, and S/C = 3. The minimum system exhaust temperature of 78 C was achieved for $U_a = 0.25$, $U_f = 0.9$, and S/C = 4.5. As fuel utilization value varies between 0.5 and 0.95 it is observed that exhaust temperature drops from 420°C to approximately 200°C. The same change in fuel

utilization also results in an efficiency increase from 30% to 42% while gross stack efficiency increases from 29% to 37%. The increase in air utilization increases net system efficiency and gross stack efficiency while decreasing the exhaust temperature. An increase in the O/C ratio results in an initial decrease in system exhaust temperature and then begins to increase. This is the same result with additional pre-heating of the mixed stream. This paper also takes into account the effect a changing S/C ratio has on the system. It is found that an increasing S/C ratio results in a rise of system efficiency and gross stack efficiency while the system exhaust temperature decreases with the increase in the S/C ratio.

There are two real sets of findings from this paper. First is that the energy from external heat sources can be avoided via thermal management of the system. This way heat recuperation is maximized and other heating requirements can be met using the heat from the afterburner exhaust, while taking heat losses into account as well.

Second, the sensitivity analysis provided insights into what to expect in terms of system performance and stack temperature when there is a change to any of: fuel type, air utilization, S/C ratio, O/C ratio, and inlet cathode temperature. This analysis has proved immensely useful.

The only real limitation identified in this study is tied to the software selected. The use of Microsoft excel, in this author's opinion, limits the analysis. Use of a fuel cell unit model can help further understand the findings of this report.

Chapter 3, in this thesis, discusses at designing a 1kW diesel-fuelled SOFC system, similar to the design of Dhingra et al., but instead of evaluating the system performance when a fuel cell unit model is used.

2.3 Ceramic Porous Burners:

With widespread environmental degradation, coupled with an increasing demand for energy, the demand for various efficient and eco-friendly energy management schemes in the industrial and residential sectors is increasing day by day. One of the technologies under consideration is combustion within porous inert media (PIM) [28]. As a self-organized process of heat recuperation, combustion in porous media is quite different from homogenous flames. This difference is attributed to the following main factors: i) the highly developed inner surface of the solid porous medium results in efficient heat transfer between the combustible medium and the inert solid; ii) dispersion of the reactant flowing through a porous media increases effective diffusion and heat transfer between the phases [29]. Thus an internal method of energy recuperation is activated. This process facilitates a combustion process that ensures stability for a wide range of reactant velocities, oxidant/fuel ratios, and power loads [30, 31]. As the combustion becomes more efficient the possibility of formation of NO_x and CO becomes minimal. A porous material means a material with connected voids, where flow can easily penetrate through the medium [32].

The basic equations governing the combustion of gaseous fuels in porous media and the resulting heat transfer modes are: energy, continuity and species conservation equations. In addition, the mathematical models of chemical reaction kinetics and radiation effects of solid and gas phases are also included [33].

In recent years many researchers have focused on developing porous media burner technology both experimentally and theoretically. Two comprehensive review papers published on this topic are: Howell et al. [34] and Kamal and Mohamed [35]. In addition Trimis and Durst's review gives an outline of advances and applications of porous media combustion [36]; whereas, Mohamed [37] provides a brief account of the fundamentals and applications of porous media combustion. Pantangi and Mishra outline the developments in matrix stabilized combustion for porous media burners [38]. Oliveria and Kaviani [39], in their study, summarize the thermal and chemical non-equilibrium processes involved in porous media combustion, its role, the innovative uses and applications, together with the current modeling of

those processes and the modeling techniques that may allow for further developments. A recent review by Wood and Harris [28] outlined the global scenario of research on lean combustion porous burners. In the present study, a comprehensive survey of the researches carried out so far in the area of porous media combustion for burners with pre-mixed and non-premixed fuel-air inlet feed is presented.

Premixed and non-premixed combustion:

Porous media combustion systems may work with a premixed flow (fuel and air been fed together through one inlet), or, more rarely, with a non-premixed fuel flow that meets a back-diffusing air flow as the fuel passes through the porous ceramic zone. Premixed porous burners consist of two sequential zones: the premixed fuel and air stream first enters a fine-pore hot solid matrix (below the flame quenching size, for safety), where it is heated until it enters the second larger-pore hotter solid matrix, where alveolar flames stabilize themselves for a wide range of flow rates and air–fuel ratios [29].

2.3.1 Pre-mixed Combustion in ceramic burners:

A porous ceramic burner has a very high radiant output due to the high emissivity of the material. The porosity provides the fuel with a complicated path through a homogeneously radiant zone, ensuring vaporization and enhancing complete reaction. Liquid fuel combustion in porous ceramics has potentially low emissions of NO_x and CO [32]. Unburned hydrocarbon and CO emissions are low due to fuel preheating and the increased residence time of exhaust gases in a high-temperature post combustion region. NO_x emissions are low due to droplet vaporization and mixing in the ceramic media. This can result in partially premixed lean combustion, which has lower flame temperatures than diffusion flames where combustion occurs at stoichiometric conditions [40].

It has been found that in burners that use premixed gaseous (as opposed to liquid) fuel-oxidizer streams, the flames ignited within the PIM (porous inert media) can be burned with leaner mixtures, higher flame speeds, and in some cases higher temperatures than can be produced in similar burners without combustion within the PIM sections [29]. Echigo [40] showed analytically and experimentally that heat recirculation from the flame to the unburned reactants could be accomplished through radiation from a porous solid.

Although not many studies have been conducted in the area of combustion in inert porous media, the results of those studies show that the combustion of premixed gas in porous media is a promising technology [41,42], revealing the presence of uniform heating zones [41] and radiative zones[43]. The following reviews the research done in the area of porous media combustion with pre-mixed fuel-air feed.

Experimental Studies Pre-mixed Fuel/Oxidant Combustion in Porous Media

Kaplan et al. [44] explores the feasibility of combusting a hydrocarbon fuel within an inert medium of high porosity. A number of studies on the combustion of gaseous fuels within porous ceramic burners have been undertaken at University of Texas Austin, Arizona State, and a number of other research institutions. A radiant burner was built, and various design configurations were tested for different ceramic material and a variety of design configurations. Porous ceramics such as: magnesia-stabilized zirconia, silicon carbide, and yitrium-stabilized zirconia were all tested. The fuel heptane was impinged on the combustion section of the system using an oil spray nozzle with a fixed flow rate. Variations of the burner were also tested including higher fuel flow rates, prevaporized fuel, and porous ceramic section. The combustion section of the burner was always insulated to prevent heat loss in all experiments.

There are a number of findings from this research that proved of some interest. First, stable combustion of a hydrocarbon fuel (heptane) within a porous ceramic media burner is possible. Yitrium-stabilized

zirconia and silicon carbide ceramics may have good resistance to thermal cycling but also come with their own set of limitations. For example, the Yitrium-stabilized zirconia (YSZ) supports complete combustion only for pre-vaporized fuels; the silicon carbine melts at the combustion temperatures experienced. It was also found that stable complete combustion for heptane was achievable at equivalent ratios of 0.57-0.67. Very low emissions of both CO and NO_x were measured for this range; it was also found that in a quartz-enclosed burner these emissions were even lower. The temperature, across the exit plane, varied by less than 50°C for the combustion section. For an equivalence ratio of 0.64 the axial temperature measurements taken down the side of the combustion zone showed temperatures of 1170-1370°C. An examination for pre-vaporized fuel found there to be little difference in CO and NO_x compared to using non-vaporized heptane.

This study showed that a commercial burner based on a ceramic porous flame stabilizer and having low emissions could have a number of very useful applications. This could include the incineration of hazardous liquid wastes. Also, such a system could be used in areas where natural gas is not available or a liquid-fuel is a by-product of an industrial process. An example of this might be in ships as a heat source for a methanol reformer, which could reform methanol into H_2 and CO of CO_2 for fuel cells to power electric vehicles. In summary, the research explored many characteristics of a liquid-fuelled porous media burner.

Ito et al. [45] conducted an experimental investigation of pre-mixed methane-air and propane-air in a porous ceramic fiber burner. Air was supplied by a blower and fuel was injected into the air supply ahead of the porous burner. The air-fuel mixture was ignited just above the burner and varying the air-to-fuel ratio controlled the size of the flame. The combustion products of the system were then released into the atmosphere. The parameters varied and tested in this study are: mixture strength, mixture velocity, and porosity of the fiber burner mat.

The results revealed the existence of five distinct stage of combustion, depending on the air ratio and velocity of the premixed feed.

Stage 1: Combustion of air-fuel mixture occurs above the burner with a luminous blue flame.

Stage 2: Combustion occurs with increasing air ratio; the luminous blue flame diminishes until it fully enters the fiber mat surface causing the surface to turn incandescent with a diffusion flame still observable above the surface

Stage 3: Further increasing the air ratio, the outer diffusion flame further diminishes until it is no longer visible. This stage is called flameless combustion stage.

Stage 4: Upon further increasing the air ratio, a blue flame, consisting of many tiny blue flames, reappears over the burner with the surface still incandescent.

Stage 5: A cellular like blue flame appears above the burner.

The most interesting of these is stage 3 where combustion is completed within the mat so that there is no flame visible above the surface – this is called flameless combustion. The temperature profile, surface temperature and profiles of CO, CO_2, and NO concentration above the surface of the porous media were also measured in this study. It was found that the temperature profile increases exponentially over the distance of porous media in the afterburner, the greater the distance – the higher the temperature. By increasing the mass flow rate into the system, it is found that emission concentration of CO decreases over the distance of the porous mat. For CO_2, on the other hand, there is a slight overall increase in the emission concentration. Transition conditions were also found to differ for propane as oppose to methane at leaned conditions. The lean flammability point of the porous burner was an air ratio of 1.9 for methane, compared to 2.16 for propane.

It has been observed that three things affect the conditions defining the combustion stage: i) the type of fuel, ii) the porosity of the material, and iii) the thermal degradation of the material. It is also found that NO_x emissions are greatly influenced by the air ratio in the system. Below follow the four criteria to be assessed in order to find optimal conditions for flameless combustion systems.

1. Completeness of combustion
2. Low emissions
3. Significant heat released as radiant energy, which can be used for other heating purposes.
4. The absence of a flame, as this results in a more compact design.

When one considers the limitations of this study, the testing of non-premixed feed in the porous ceramic fiber has not been explored.

Yumlu et al. [46] studied hydrogen-oxygen and hydrogen-air combustion in a porous flat flame burner with heat extraction. The temperature of these two flames was determined experimentally and compared with calculated thermodynamic values to measure the heat loss to the burner. The hydrogen concentration across the burner was measured using a quartz microprobe and mass spectrometer. W.E. Kaskan's technique was used to measure the flame temperature at the center of the burner [47]. The flame temperatures were calculated by measuring the enthalpy of the initial mixture, estimated using the standard thermodynamic data and the heat loss to the burner.

There were three major findings in this paper that were relevant to this work. First, the data shows that as burning velocity decreases, heat released first increases and then decreases, resulting in a critical burning velocity. Second, when this critical burning velocity is reached, the heat released is highest, in line with the prediction of thermal conductivity of inflammability limits. Finally, it was found that the error between calculated and measured temperatures can be reduced by eliminating heat transfer across the

burner to the atmosphere. Therefore, the true magnitude of the critical burning velocity can be calculated using a shielded adiabatic burner.

There have been two similar studies on this topic of note: Trimis and Durst [36], and Durst et al. [48]. The main focus of their work was the combustion stabilization principle, to allow for a stable combustion reaction in a porous matrix using pre-mixed feeds. They both found that changing the pore size (and the Peclet number in turn) helps to stabilize the combustion and flame.

A major limitation of these studies is that it only discusses pre-mixed feeds. Further, the effects of change in the equivalence ratio are not discussed.

Rortveit et al. [49] compares the combustion of lean pre-mixed fuel mixtures of methane and hydrogen in four different NO_x burners. The four burners include a fiber burner, a swirl burner, and two inert porous media burners, one with, and the other without, catalytic support. The concentration of CO, CO_2, NO_x, and O_2 are the measured outcome variables. The two porous media burners are designed for premixed operation at high excess air ratios. Al_2O_3/SiO_2 is used as ceramic fibers for the porous burner, which have high heat transports. The catalytic supported porous burner has a ceramic honeycomb region with an alumina based wash coat of Pt and Pd as catalysts.

It was found that the NO_x and CO emissions were dependent on the type of burner and equivalence ratios. Hydrogen when mixed with CH_4 was beneficial in creating stable combustion in the porous media burners. Furthermore, in this study it is stated that the porous media burners had very low pressure drops in addition to achieving low emissions of NO_x and CO, when run on excess air ratios. Finally, it was observed that high turndown ratios and burning mixtures with lower calorific values are beneficial in porous media burners, as the burner shows better system efficiencies and also low CO emissions

This paper makes the point that using porous media for gas turbines and industrial boilers is effective for the reduction of pollutants from these combustion applications. It is also shown that mixing H_2 in the fuel

feed makes the thermal reactions in porous media burners more stable. Finally, the lower NOx emissions can be achieved without the necessity of high excess air ratios.

Modelling Studies of Combustion in Porous Media

Mujeebu et al. has published a comparative review of the various modeling approaches that have been used for porous media combustion [50].

Takeno and Sato [51] have proposed a model that can be used to study the effects of mass flow rate and heat transfer coefficient on flame characteristics in excess enthalpy flames. They suggest that inserting a porous highly conductive solid will conduct heat from the solid to the reactants. The inserted porous solid produces the excess enthalpy distribution extending around the solid inlet, which in turn brings about the characteristic temperature profile in the gas flow with a peak that is higher than adiabatic flame temperature. The reaction is almost completed at the porous solid exit. Takeno et al. also developed a modified model to investigate the effects of finite length of porous solid; they discovered a critical mass flow rate beyond which the flame was no longer self-sustaining. Beyond this critical flow rate the flame extinguished, this flow rate changed with the configuration of the combustion system, in particular the length of the solid and heat loss system were determinant factors. Chen, who was a coworker with Takeno, extended their earlier work on critical mass flow with this new extended model

Chen et al. [54] applied the energy and species conservation equations to model porous media burners. A multi-step mechanism for methane combustion based on the reaction set of Kee et al. [56] was used. The mechanism included 17 species and 55 reactions. Thermal conductivity of the porous solids, the volumetric heat transfer coefficients, and the radiative heat transfer properties were all varied over typical ranges in order to determining their effect on flame speed and temperature profiles. A high local heat transfer coefficient was used, and it was assumed that the solid and gas temperatures were locally equal,

simplifying the solution to only one energy equation. This assumption, however, was removed in the subsequent study where the more complete multiple step reaction kinetics replaced the single-step mechanism. The critical flow rate was dependent upon the type of combustion system; particularly the length of the solid and the heat losses in the system.

Echigo [53] investigated the effectiveness of the radiant heat transfer from a porous media that was being heated by a stream of non-reacting hot gases. Following this, Echigo and his co-workers developed a rigorous model for multi-mode heat transfer by using a single-step reaction model for the combustion of H_2-CH_4 gas mixture with an Arrhenius rate constant and the exact solution for radiative transfer in the heat absorbing / emitting medium. The burner was divided into three regions: i) upstream – where no reactions occur, ii) a combustion zone, and iii) an exit zone where the gases leave the combustion zone and undergo no further reaction. Based on this set of assumptions they were able to predict, temperature profiles for the gas flow through the porous media, well.

2.3.2 Non-premixed porous media combustion:

The development of a commercially successful flat surface porous radiant burner, using non-premixed feed, would be of great benefit to the energy industry. Only few works have been completed with the aim of informing the design of such a burner. Current porous media burners under development are limited by their turndown ratio, as well as problems with flame stability, which leads to flashback [56]. For these burners, at high flow fuel rates, the flames may amplify. Therefore these burners must operate in the low velocity regime where mixing between fuel and air is primarily due to molecular diffusion. As a result, the maximum combustion rate of these burners is usually quite low [57].

Kamal and Mohamed [37], investigated how to enhance the radiation flux for a porous media burner that was operating with non-premixed flames by using a vane-rotary burner. The air duct confines the swirling

flow in the rotary burner. There are three major findings from this paper that are of interest. First, the enhancement in flame radiation output with a swirl that was 1.9 times greater than without swirl simulation. In addition to this, inserting a porous medium at the burner exit enhanced the radiation output to 4.18 times while promoting droplet evaporation at the exit. Finally, the paper explains that an enlarged recirculation zone beneath the fuel injector while introducing a porous medium for non-premixed input streams increased combustion efficiency of the overall system.

There are two major limitations to this study. First, there was very little information or analysis provided on the porous media burner with a non-premixed feed and an overemphasis on radiation flux enhancement. Second, there was no information about testing the effect a pre-mixed feed would have on radiation flux.

It must be noted that Meng et al. [58] also conducted a similar study to discuss the effects of porous media inserts with non-premixed feed. The study found a 60% enhancement in the performance of a water heat exchanger with ceramic inserts if a non-premixed feed was passed through. A reduction in NO_x level by a factor of 3 was attributed to the efficient heat removal from exiting gases. It was also found that the finest porosity with the highest surface area-volume ratio yielded the highest efficiency while lowering the porous matrix deeper into the combustion zone worsened the efficiency. It also points out that convective heat transfer from gas to solid is effective only once the fuel energy is released as pure thermal energy.

Mital and Gore [59] in their paper, study laminar diffusion flames and how they are affected by either the presence or absence of ceramic porous media. The researchers discovered that when porous media is present there was a 65% enhancement of radiative flux. It also states that there was an increase in CO and hydrocarbon emissions at low flow rates due to chemical reactions in the pre-ceramic region. Above a certain flow rate and positioning of the ceramic porous media emissions reduced the CO and hydrocarbon emissions. The paper also notes that effective air-fuel mixing should occur before the porous zone to

prevent quenching of the porous media. Combustion engineering is also driven by the position of porous media in the combustion zone.

Hall et al. [57] designed a prototype non-porous radiant burner with non-premixed methane-air combustion for experimental testing. The prototype used small diameter tubes to bring in methane via a convection air stream and is made of silicon carbide. The methane air is locally mixed near the exit tubes right below the porous ceramic section. Combustion begins slightly before the porous zone and continues within the zone itself. A manifold system was designed to separate the fuel and air prior to mixing.

This paper presented quite a few interesting findings since a large range of flow rates and air levels were studied. The burner operated with fuel enthalpy inputs from 1.2kJ/hr/cm^2 to 5.6kJ/hr/cm^2, based on lower heating value. The experiments were first conducted with no space between the flow tubes and porous matrix. It was discovered that some combustion occurred within the ceramic matrix, while a diffusion flame exited from the porous zone and some combustion was completed beyond the porous zone. This slight overflow of combustion was typical for most flow rates and excess air levels examined. When the experiment was repeated with a gap between the tubes and porous matrix most of the combustion reaction occurred in this gap creating a relatively turbulent blue flame.

It was learnt from this paper that no flashback was observed during any experimental run. The characteristics of the combustion were affected by the flow rate. At low flow rates, the flame is more yellow and it shifts towards blue as the flow rate increases. For air levels in excess of 120% the ceramic had a strong reddish-orange glow, indicating a significant radiative heat transfer. This glow is usually found in pre-mixed ceramic burners' combustion of methane. Throughout these tests the ceramic was also found to hold up well to any combustion reaction with no visible wear and tear.

The only observable limitation of this study is that the radiant output, emission concentrations, and temperature profiles were not made available for the experimental runs, in this paper.

Chapter 4 analyses design work of a ceramic tail-gas burner for a 1kW diesel fuelled SOFC system, which has been experimentally tested and designed at NRC-IFCI. The chapter discusses non-premixed ceramic burner combustion.

Works Cited

[1] Shekhawat, D. (2011). Introduction to Fuel Processing. In D. Shekhawat, *Fuel Cells, Technologies for fuel processing.* Amsderdam: Elsevier.

[2] Peng. H. (2004). Control of fuel cell power systems: principles, modeling, analysis, and feedback design. London: Springer.

[3] Speight J, (2011). The Biofuels Handbook, RSC Publishing.

[4] Naidja A, K. C. (2003). Cool flame partial oxidation and its role in combustion and reforming of fuels for fuel cell systems. Energy Combustion Science, 155-191.

[5] Rostrup-Nielsen JR, C. L. (2011). Concepts in Syngas Preparation. London: Imperial College.

[6] Rostrup-Nielsen, J. (2002). Large Scale Hydrogen Production. 150 – 159

[7] Qi A, W. S. (2005). Autothermal Reforming of n-octance on Ru-based catalysts. 71-82.

[8] Pors Z, P. J. (2008). Optimized mixture formation for diesel fuel. Fuel Cells, 129-137.

[9] O'Connell M, K. G. (2009). Development and evaluation of a microreactor of diesel fuel in the kW range. Hydrogen energy, 290-303.

[10] Moon DJ, S. K. (2001). Studies on gasoline fuel processor system for fuel cell powered vehicles application. 1-9.

[11] Rostrup-Nielsen JR. (1984). Steam Reforming. In Anderson JR, Catalysis, science and technology, vol 5 (pp. 100-117). Berlin: Springer-Verlag.

[12] Rostrup-Nielsen JR. (1993). CO2 reforming of methane over transition metals. 38-49.

[13] Andrew SPS. (1969). Catalysts and catalytic processes in the steam reforming of naphtha. 321-324.

[14] Gangwal, S. (2011). Desulphurization of fuel cells. In D. Shekhawat, Fuel Cells: Techonologies for Fuel Processing (pp. 325-350).

[15] Babich IV, M. J. (2003). Science and technology of novel processes for deep desulphurization of oil. 607631.

[16] Lawrence, J., & Boltze, M. (2006). Auxillary Power unit based on a solid oxide fuel cell and fuelled with diesel. *Jounal of Power Sources*, 479-488.

[17] Zizelman, J. (2000). Solid oxide fuel cell auxillary power unit-A paradigm in electric supply for transportation. 70.

[18] Stelter, M. (2006). Engineering Aspects and hardware verification of a volume producible solid oxide fuel cell stack design fore diesel auxillary power units. *Journal of Power Sources*, 448-455

[19] Roychoudary, S., & Lyubovsky, M. (2006). Design and development of a diesel and JP-8 logistic fuel processor. *Journal of Power Sources*, 510-513.

[20] Lyubovsky, M., & Roychoudary, S. (2005). Catalytic partial oxidation of methane to syngas at elevated pressures. 113-117.

[21] Lisbona, P., & Corradetti, A. (2007). Analysis of a solid oxide fuel cell system for combined heat and power applications under non-nominal conditions. *Electrochimica Acta*, 1920-1930

[22] Zink, F., & Lu, Y. (2007). Energy Conv. 809.

[23]Costamagna, P., & Magistri, L. (2001). Design and part-load performance of a hybrid system based on a solid oxide fuel cell reactor and a micro gas turbine. *Journal of Power Sources*, 352-368.

[24] Yi, Y., & Rao, A. (2005). Fuel flexibility study of an integrated 25kW SOFC reformer system. *Journal of Power Sources*, 67-76.

[25] Singhal, S. (2000). Advances in solid oxide fuel cell technology. *Soli State ionics*, 305-313.

[26] Skrivan, W. (2002). *Parametric testing and analysis of a 25kW SOFC system.* Irvine: Department of Mechanical and Aerospace Engineering, University of California.

[27] Dhingra, H., & Peppley, B. (2013). Sensitivity Analysis of a 1kW diesel-fuelled SOFC generator: A single and paired variable study. *Journal of Power Sources*, 1-11.

[28] Wood, S., & Harris, A. (2008). Porous Burners for lean burn applications. *Progress in energy and combustion science*, 667-669.

[29] Mujeebu, A., & Abdullah, M. (2009). Combustion in Porous media and its applications. *Journal of Environmental Management*, 2287-2312.

[30] GoGas. (n.d.). *Porous Burner Radimax*. Retrieved July 2013, from www.hohas.de

[31] Promeos. (n.d.). *Porous Burners*. Retrieved July 2013, from www.promeos.coms

[32] Pickenacker, O., & Trimis, D. (1999). Application of the porous burner technology in energy and heat engineering. *Proceedings of the fifth international conference on technologies combustion for a clean environment*, (pp. 519-523). Lisbon.

[33] Rumminger, M. (1996). *Numerical and experimental investigation of heat transfer and pollutant formation in porous direct-fired radiant burners.* Berkeley: PhD thesis, University of California.

[34] Howell, J., & Hall, M. (1996). Combustion of hydrocarbon fuels within porous inert media. *Progress in Energy and Combustion Science*, 121-145.

[35] Kamal, M., & Mohamed, A. (2006). Combustion in porous media, a review. *Journal of Power and Energy*, 487-508.

[36] Trimis, D., & Durst, F. (1996). Combustion in a porous medium – advances and applications. *Combustion Science and Technology*, 153-168.

[37] Mohamed, A. (2005). Combustion in porous media: fundamentals and application. In *Transport Phenomena in Porous Media III* (pp. 287-304).

[38] Patanghi, V., & Mishra, S. (2006). Combustion of gaseous hydrocarbon fuels within porous media. *Advances in Energy Research*, 455-461.

[39] Oliveria, A., & Kaviani, M. (2001). Nonequilibrium in the transport of heat and reactants during combustion in porous media. *Progress in Energy and Combustion Science*, 523-545.

[40] Echigo, R. (1983). Combustion augmentation of extremely low calorific gases: application of the effective energy conversionmethod from gas enthalpy to thermal radiation. *Proceedings of the ASME–JSME Thermal Engineering Joint Conference*, (pp. 99-104). Honolulu.

[41]Bito, T. (1989). *Proceeding on the 27th Symposium on Combustion*, (p. 329).

[42] Tong, T. (1990). *International Journal of heat mass transfer*, 1339.

[43] Kuwahara, S. (1989). 45.

[44] Kaplan, M., & Hall, M. (n.d.). The Combustion of Liquid Fuels within a Porous Media Radiant Burner. *Centre of energy Studies, Department of Mechanical Engineering, The University of Texas at Austin*.

[45] Ito, K., & Fujita, O. (1991). Flameless Combustion within Porous Radiant Burners using Ceramic Fiber Mat as burner material. *Bulletin of the Faculty of Engineering*, 51-60.

[46] Yumlu, V. (1966). Temperatures of flames on porous burners. *Combustion and Flames*, 147-151.

[47] Kaskan, W. (1957). *Sixth Symposium on Combustion.* New York: Reinhold.

[48] Durst, F. (1997). Der Porenbrenner–Konzept. *Technik und Anwendungsgebiete*, 300-307.

[49] Rortveit, G. (2002). a comparison of low-nox burners for combustion of methane and hydrogen mixtures. *Proceedings of Combustion Institute*, 1123-1129.

[50] Mujeebu, M., & Abdullah, M. (2010). Trends in modelling of porous media combustion. *Progress in Energy and Combustion Science*, 627-650

[51] Takeno, T., & Sato, K. (n.d.). A theoretical study on an excess enthalpy flame.

[52] Takemo, T. (1986). Dynamics of reactive systems Part 1: flames and configuration. *AIAA ProgAstronaut Aeronaut*, 246-262.

[53] Echigo, R. (1982). Effective energy conversion method between gas enthalpy and thermal radiation and application to industrial furnaces. *Proceedings of 7th International Hrat Transfer Conference*, (p. 361). Munich.

[54] Chen, Y., & Matthews, R. (1987). The effect of radiation on the structure of a premixed flame within a highly porous inert medium, in radiation, phase change heat transfer and thermal systems. *ASME publications vol 81*. 35-42.

[55] Kee, R., & Milller, J. (1980). *CHEMKIN:A general purpose problem independant, transportable chemical kinetic reaction.* Sandia National Laboratory.

[56]Evans, W. (1991). *Experimental Stability Limits of Methane Combustions inside a Porous Ceramic Matrix.* MS Thesis, Deparment of Mechanical Engineering, The University of Texas, .

[57] Hall, M. (1993). A porous ceramic radiant burner utilizing non-premixed combustion of gaseous fuels. *Proceedings of the Joint Techincal Meeting on Combustion Fundamentals and Applications*, (pp. 699-702). Wisconsin.

Hall, M. (1993). A Porous Ceramic Radiant Burner utilizing non-premixed combustion of gaseous fuels., (pp. 699-702).

[58] Meng, W., & McCordic, C. (1991). A study of effects of porous inserts on heat transfer and combustion in fired heat exchanger. *Proceedings of 1991 ASME/JSME Thermal Engineering Joint Conference*, (pp. 181-188). Maui.

[59] Mital, R., & Gore, J. (1994). An experimental study of laminar diffusion flames with enhanced heat transfer by reticulated ceramic inserts. *ASME Heat Transfer Fire Combustion Systems*, 31-39.

Roychoudary, S., Lyubovsky, M., & Ahmed, S. (2005). Microlith catalytic reactors for reforming iso-octane-based fuels in hydrogen . *Journal of Power Sources*, 75-86.

Chapter 3

System Model of a 1kW SOFC Diesel Generator

3.1 Process Description:

In this chapter, analysis of a 1kW diesel-fuelled SOFC system at steady-state conditions is presented. This model is an improvement of the model presented by Dhingra et al. [1], as this model uses a preprogrammed fuel cell unit operation, which had recently been developed by technicians at VMGSim™. The fuel cell in the diesel-fuelled SOFC system developed by Dhingra [1] is defined by a custom built Microsoft excel worksheet, where all the mass and energy balances are put in as equations in the worksheet [1]. Further details explaining the setup of the newly developed unit operation are discussed in section 3.2.

An auto-thermal reformer is selected for this fuel cell system, since the heat requirements in the reformer can be controlled by changing the amount of fuel, steam and air allowed in the reactor. Auto-thermal reforming is usually limited for use in auxiliary power units. Other than Dhingra et al., the literature reviewed on diesel-fuelled systems, shows that most SOFC systems either use steam reforming or catalytic partial oxidation reforming for their fuel processors [6-10].

The tail-gas burner exhaust serves as the primary heating utility for the system. The availability of heat in the system for heat recovery from the Afterburner exhaust avoids the need for an auxiliary heat source. A heat exchanger system is also implemented in this fuel processor system to maximize heat utilization in the system and improve the overall system efficiency. All the heat exchangers are counter-current, enabling lower approach temperatures within the exchangers.

Steam mixers and splitters are used to mix steam and air flows, as well as dividing these streams into cathode stream and reformer streams. In addition to these components, desulphurization unit, blowers and fuel and water pumps are also used for in the SOFC system simulation.

A sensitivity analysis was conducted to determine the influence of key process parameters, such as S/C ratio and O/C ratio. The output variables measured: i) net system efficiency, and ii) stack efficiency.

.

3.1.1 Assumptions:

The fuel composition chosen for the diesel fuel is similar to the fuel composition used by Dhingra et al. [1] in his SOFC system. Table 1 shows the composition of the simulated diesel fuel used as the feed to the system.

Table 1: Mole Fraction of Higher Hydrocarbons in Diesel Feed [1]

n-nonane	0.0151	n-hexylbenzene	0.05692
n-decane	0.0084	n-heptylbenzene	0.04607
n-undecane	0.00434	n-octylbenzene	0.0472
n-dodecane	0.00264	n-nonylbenzene	0.04984
n-tridecane	0.00132	n-decylbenzene	0.04833
n-tetradecane	0.00142	n-undecylbenzene	0.11148
n-pentadecane	0.00312	n-dodecylbenzene	0.17727
n-hexadecane	0.00661	Naphthalene	0.06136
n-heptadecane	0.01416	1-methylnaphthalene	0.00312
n-octadecane	0.03002	1-ethylnaphthalene	0.005
n-nonadecane	0.06334	1-propylnaphthalene	0.00765
n-eicosane	0.13112	1-n-butylnaphthalene	0.01237
n-pentylbenzene	0.07901	Phenyl mercaptan	0.0128

Some of the assumptions made while designing the system are given below:

1. Pressure drop is either assumed negligible or given a value (approximately 0.5-2.5kPa) across components throughout the system.
2. The auto-thermal reformer and the tail-gas burner are modelled as Gibbs reactors, hence they are assumed to be adiabatic. The heat input to both reactors is zero.
3. Similar to the SOFC system used by Dhingra et al. [1], the desulphurizer unit in this system is a liquid adsorption single separator. The efficiency of the desulphurizer unit is assumed to be 100%
4. Water gas shift reaction occurs in the reformer; hence CO reacts with steam to produce H_2 and CO_2 on a stoichiometric basis.
5. CO does not oxidize in the fuel cell stack because mass transfer of CO into the TPB region is about 10 times slower than H_2 [1].
6. H_2 oxidation is pre-dominant in the fuel cell stack
7. The catalytic surface area in the reformer is higher for oxidation reaction than at the TPB boundary [1]
8. The leftover CH_4, H_2 and CO is burnt in a ceramic porous afterburner.
9. No carbon deposits are formed.

3.1.2 Definitions:

The net system efficiency is defined as the net power output over the lower heating value (LHV) of the fuel entering the system. The parasitic losses ($W_{parasitic}$) are incurred from additional power requirements in the system such as the air compressor and heaters that would need to be supplied by the stack. From literature it is found that Lower Heating Value (LHV) can be approximated to be 42.3MJ/kg [3, 11].

$$\boldsymbol{eff_{sys}} = \frac{\boldsymbol{W_{elec} - W_{parasitic}}}{\boldsymbol{m_{fuelin} \times LHV_{fuelin}}} \quad \text{(Equation 6)}$$

In this case, the stack efficiency and the power output has been calculated by the fuel cell unit operation available in VMGSim™.

The reformer efficiency is defined as the ratio of the LHV of the anode feed gas to the stack over the LHV of the fuel feed to the ATR. The LHV is based on the CH_4, CO and H_2 content of the anode feed gas. CH_4, CO and H_2 are the only combustible species in the anode feed.

$$eff_{ATR} = \frac{m_{CO}LHV_{CO}+m_{H2}LHV_{H2}+m_{CH4}LHV_{CH4}}{m_{reffuel}LHV_{reffuel}} \quad \text{(Equation 7)}$$

3.2 Fuel Cell unit Operation:

Given the characteristics of the system and the type of fuel cell stack currently available at the NRC-IFCI where the system was to be implemented, it was decided that a planar solid oxide fuel cell be used. The proposed stack design of the fuel cell is shown in Figure 4.

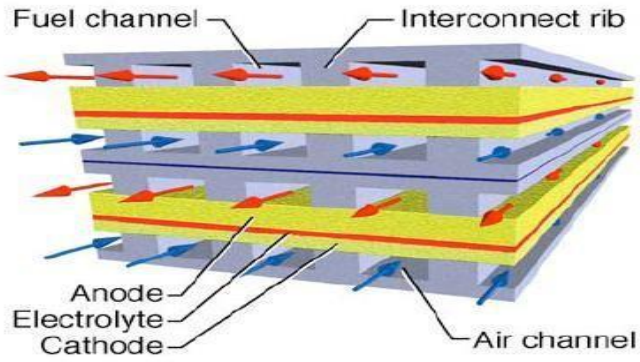

Figure 4: SOFC stack design (Taken from Solid-oxide fuel cells (SOFC) with hydrocarbon and hydrocarbon-derived fuels [5])

The air and fuel flow is counter current within the stack. The air flows on the cathode side of the cell through the interconnect ribs, while fuel flows through the anode side of the cell. An electrolyte is found between the anode and the cathode of the cell. The O_2 from the air is reduced at the cathode and is transported through the electrolyte by ionic conduction to the anode where it reacts with hydrogen on the fuel side and releases two electrons per water molecule formed. The overall process is described by the following reactions:

$$1/2O_2 + 2e^- \rightarrow O^{2-}$$ (Equation 8)

$$H_2 + O^{2--} \rightarrow H_2O + 2e^-$$ (Equation 9)

The movement of the electrons from the anode back to the cathode produces an electrical current external to the cell and stack.

For a given current density, cell temperature and species composition, the output voltage for a cell can be calculated using basic thermodynamics and correlations for the associated polarization losses incurred due to activation, ohmic and mass transport overvoltage losses. The VMGSim™ fuel cell unit operation is an implementation of such a model and the beta version that was made available for this work was effective for analyzing the performance of a 1 kW SOFC system.

3.2.1 Unit Operation Setup:

Figure 5 below shows the initial trial that was conducted to test the fuel cell unit operation.

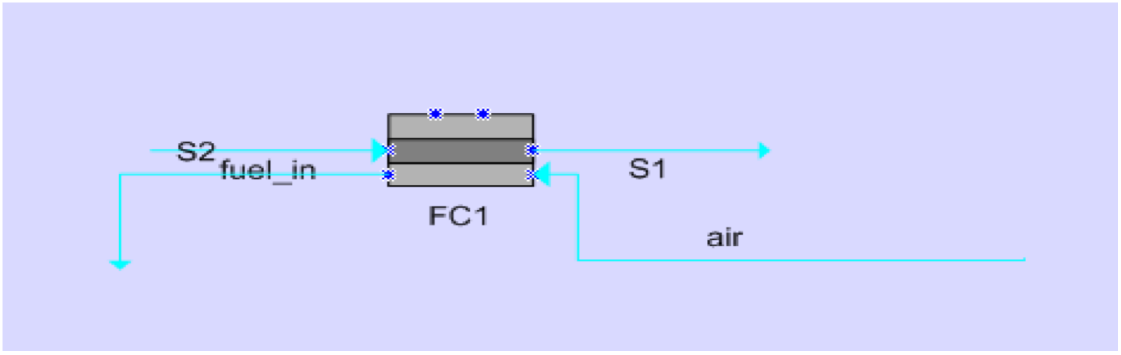

Figure 5: Initial testing set-up for the fuel cell unit operation

The inlet compositions of hydrogen, methane and carbon monoxide as well the inlet flow rate were arbitrarily specified at typical values in this case, as the fuel cell unit operation was being initially tested. Figure 6 shows the input screen of the operational parameters required to set up the unit operations.

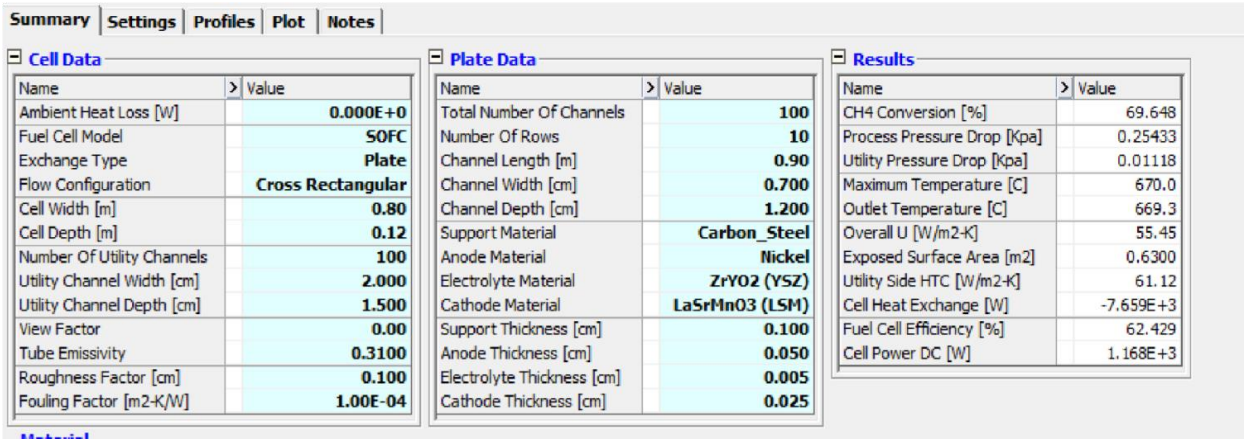

Figure 6: Operational Data for fuel cell unit operation

Some of the parameters that are required in setting up the fuel cell unit operation are: i) type of fuel cell model and its flow configuration, ii) dimensions of the cell and plate, and iii) characteristics of the materials used.

Once the key parameters are set the fuel cell unit operation calculates the fuel cell stack voltage and efficiency. The DC power output produced by the fuel cell stack, for given parameters, is also calculated. Other results that are calculated include: i) methane conversion, ii) stack and outlet temperature, and iii) pressure drop.

3.3 Model Analysis:

Modeling of the 1kW diesel fueled SOFC system was conducted using the Peng-Robinson (PR) fluid package. The model is ideal for vapour/liquid equilibrium calculations as well as for calculating liquid densities of hydrocarbon mixtures. Equilibrium conditions were assumed for the product streams from the reformer, SOFC and afterburner. Convergence problems were initially encountered for the heat exchanger system and the fuel cell unit operation but once a converged solution was achieved, small

incremental changes in the operating conditions resulted in relatively rapid convergence to a solution that showed consistent trends.

3.4 Process Design

One of the main goals of this modelling effort was to develop fuel processor specifications for a 1kW diesel-fuelled SOFC power system. Operational data and component specifications that were available for a biogas-fuelled SOFC system that was developed at the National Research Council Institute for Fuel Cell Innovation (NRC-IFCI) in Vancouver were used as a reference source and starting point.

3.4.1 Process Flow Diagram:

Figure 7 shows the process flow diagram for the simulation. Diesel is fed to the system, at room temperature. Heat exchanger (HX4) is used to vaporize the diesel.

The mass flow rate of the inlet diesel feed was 0.2596 kg/hr. (See Appendix A.1 for calculations). The water and air feeds are also at room temperature and atmospheric pressure. The oxygen to carbon ratio for this system is 0.31 and the steam to carbon ratio is 2.25 [2]. Table 2 shows the inlet feeds and their mass flow rates.

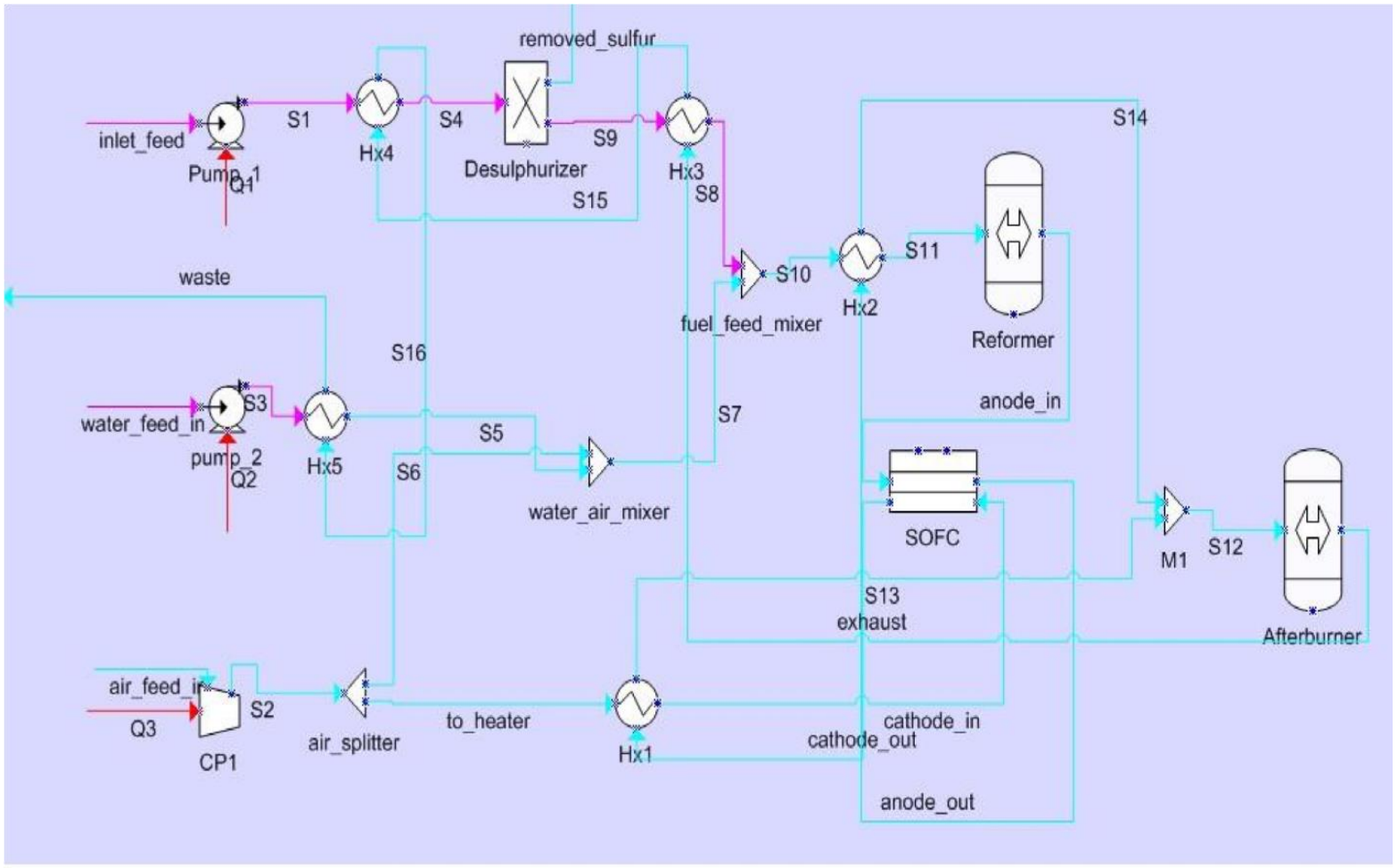

Figure 7: PFD diagram of a 1kW SOFC system with diesel as fuel

Table 2: Mass flow rate of inlet feeds

Feed	Mass flow rate (kg/hr)
Diesel	0.2596
Water	0.89
Air	8.10

3.4.2 Base Case Performance:

Desulphurizer:

After vaporizing the diesel, the stream (S4) enters the desulphurizer. This is a single stage component separator which is used as a desulphurizer to remove all H_2S in the stream. It is a liquid adsorption separator and the efficiency of sulphur removal is set to be 100%. Desulphurization is required upstream of the stack and reformer as sulfur is known to be harmful to the fuel cell anode and reformer catalyst.

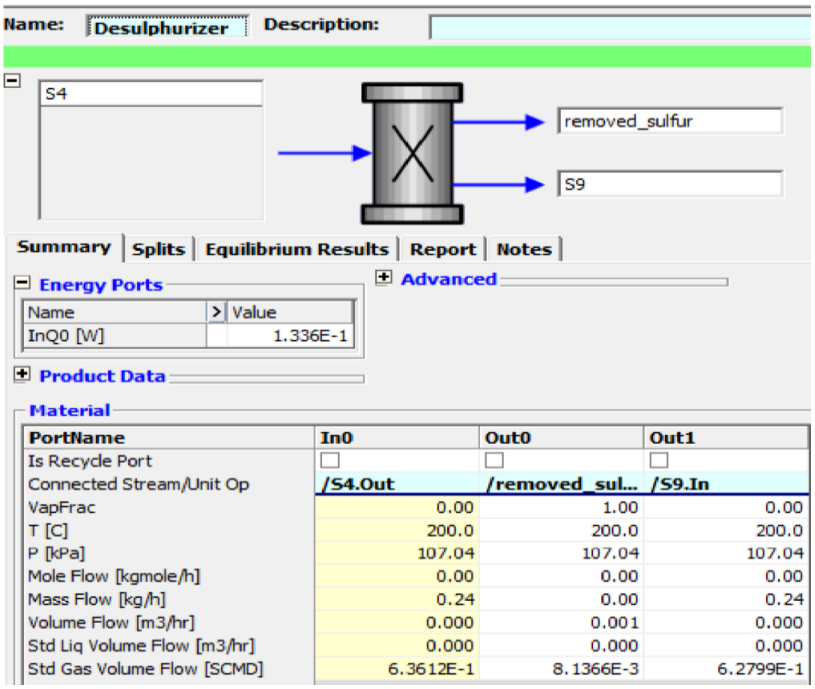

PortName	In0	Out0	Out1
Is Recycle Port	☐	☐	☐
Connected Stream/Unit Op	/S4.Out	/removed_sul...	/S9.In
VapFrac	0.00	1.00	0.00
T [C]	200.0	200.0	200.0
P [kPa]	107.04	107.04	107.04
Mole Flow [kgmole/h]	0.00	0.00	0.00
Mass Flow [kg/h]	0.24	0.00	0.24
Volume Flow [m3/hr]	0.000	0.001	0.000
Std Liq Volume Flow [m3/hr]	0.000	0.000	0.000
Std Gas Volume Flow [SCMD]	6.3612E-1	8.1366E-3	6.2799E-1

Figure 8: Operational values of inlet and outlet feeds of a desulphurizer

Reformer:

After the diesel feed has been desulphurized, it is pre-heated to 300°C by HX3 (heat exchanger). The diesel vapour is then mixed with the air and water feed (S10 in Figure 7) and again heated by HX2 (heat exchanger), raising the inlet temperature of feed (S11), into the reformer, to 610°C. The temperature of S11 (Figure 9) was kept above 600°C, to avoid carbon formation and drive the reaction kinetics in the reformer so that sufficient heat is generated for the steam reforming reaction. The air flow, mixed in the feed was controlled, so that just enough oxygen is provided to keep the auto-thermal reformer at the desired temperature. The reformer is kept under adiabatic conditions; hence no energy stream has been connected to the reformer in Figure 9. The reactor is set as a Gibbs reactor meaning that the exit stream is at equilibrium with respect to all species. Figure 9 shows the reaction and the production of hydrogen in the reformer. It should be noted that all the higher hydrocarbons react to form either hydrogen or methane.

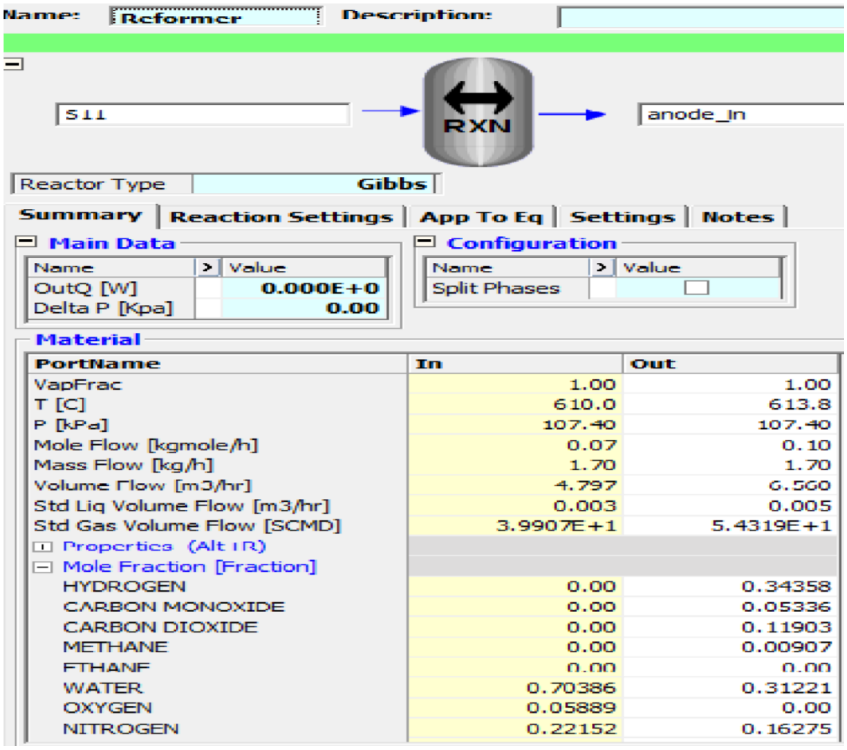

Figure 9: Operational Data of the Auto-thermal Reformer

Fuel Cell:

Based on a series of exploratory tests of the fuel cell unit operation, a set of operating parameters to evaluate the performance of the base case diesel fuelled SOFC system was established. The dimensions of the individual fuel cells in the stack were based on values from literature [2]. For this scenario, it was arbitrarily assumed that there was no heat loss from the fuel cell stack. This is a reasonable assumption as the entire stack and fuel processor assembly is typically contained in a hotbox such that the difference in temperature between the outside of the stack and its surroundings is less than 40°C. Table 3 and Table 4 provide information about the dimensions of the stack, material used, as well as the results collected for the fuel cell stack used for this case.

Table 3: Operational data for the fuel cell unit operation

Stack and Cell Settings			
Flow Configuration	Cross Rectangular	SOFC Pressure [Pa]	105000
Support Material	Carbon steel	SOFC single cell voltage [V]	0.75
Anode Material	Nickel	Cathode inlet temperature [K]	800
Electrolyte Material	ZrYO2 (YSZ)	Anode inlet temperature [K]	613.8
Cathode Material	LaMnO3	Anode thickness [µm]	20µm
Roughness Factor [cm]	0.1	Cathode thickness [µm]	500
Tube Emissivity	0.31	Electrolyte thickness [µm]	20
S to C ratio	2.25	Support thickness [µm]	500
O2 to C ratio	0.31	Cell Length [cm]	1
Cell Area [m2]	100	Number of cells	100

Table 4: Results produced by the fuel cell unit operation

Name	**Value**
Methane Conversion [%]	99.988
Process Pressure Drop [kPa]	0.00656
Maximum Temperature [^{o}C]	969.2

Cathode Outlet Temperature [^{o}C]	969.2
Anode Outlet Temperature [^{o}C]	923.0
Overall U [W/m2-K]	18.96
Cell Heat Exchange [W]	392.8
Fuel Cell Efficiency [%]	62
Cell Power DC [W]	1200

Table 4 shows that the outlet temperature of the anode feed out is 923°C. Since only 9.7% of the inlet feed to the anode is methane, this methane is converted through internal reforming in the SOFC. The fuel cell efficiency of the SOFC is calculated to be 62%. The overall power produced by the SOFC is shown to be 1200W, which indicates that the mass flow rate and the oxygen to carbon ratio used earlier in the calculation are accurate.

Afterburner:

The purpose of an SOFC afterburner is to provide heat for maintaining the operating temperature, vapourizing water and diesel, as well as providing heat for reforming. Traditionally, the afterburner oxidizes the combustibles in the exhaust fuel by combining it with the exhaust air. In this case, the cathode_out and anode_out are mixed together and fed to the Afterburner. Excess hydrogen and carbon monoxide are converted to water and carbon dioxide. Figure 10 shows the operational data and compositions of the inlet and outlet feeds from the Afterburner.

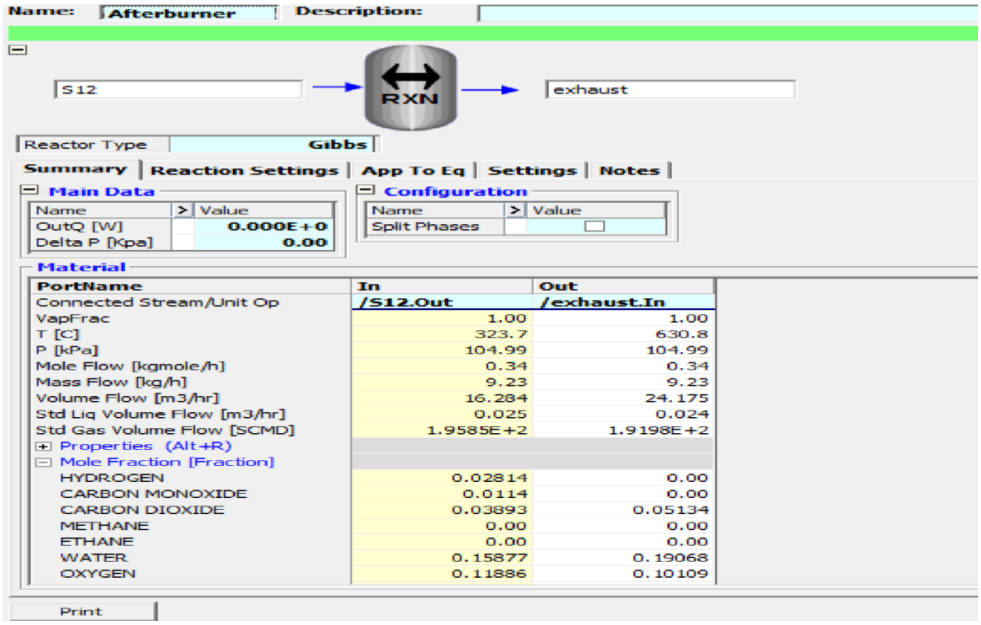

Figure 10: Data of the Afterburner

There are two scenarios available while setting up the afterburner. First, for the afterburner the outlet temperature is controlled at 1000°C. The thermal energy produced by the Afterburner, in this case, is approximately 780W. This energy is sufficient to vaporize water and diesel feeds, by running the outlet feed of the Afterburner through the heat exchanger network. In the second scenario, the outlet temperature is controlled by making it an adiabatic reactor. The outlet temperature is found to be approximately 630°C. It should also be noted that all the hydrogen is converted and no carbon monoxide is present in the outlet stream.

3.4.3 System Efficiency:

The stack efficiency and the power output were calculated by the fuel cell unit operation. The fuel cell is reported to be approximately 62% efficient and produces 1200W of DC power (Refer to Table 4). The Afterburner produces 780W of thermal energy, which is used to vaporize the diesel and water feed,

through the heat exchangers. The parasitic load, in this case, comprises of the energy provided to pumps, blowers and compressors.

Table 5 shows the values used to predict the system efficiency using the equation 6.

Table 5: System Efficiency

	Values
$\mathbf{W_{elec}}$	1200W
$\mathbf{W_{parasitic}}$	37W
$\mathbf{m_{fuelin}}$	0.24kg/hr
LHV	42.3MJ/kg
System efficiency	41.2%

A predicted system efficiency of 41% is within the range of 30 – 45% found in the literature, while taking parasitic losses and heat losses from the heat exchanger network, into account [3]

3.5 Sensitivity Analysis:

The sensitivity of the net system efficiency and stack efficiency to several process variables was studied.. Two operating variables were studied:

- Oxygen to Carbon ratio in Feed
- Steam to Carbon ratio in Feed

Although it would have also been interesting to investigate the sensitivity of the system performance to changes in air and fuel utilization, the configuration of the fuel cell unit operation was such that adjusting

the utilization required a lengthy iterative process to reset the feed rates so that the overall output power of the system was maintained at 1 kW.

3.5.1 Effect of Varying O_2 / C ratio:

The molar flow rate of air entering the system was determined by the $O_2$to C ratio and the diesel fuel feed rate. Figure 11 shows the change in net system and stack efficiencies with the increasing O_2 to C ratio.

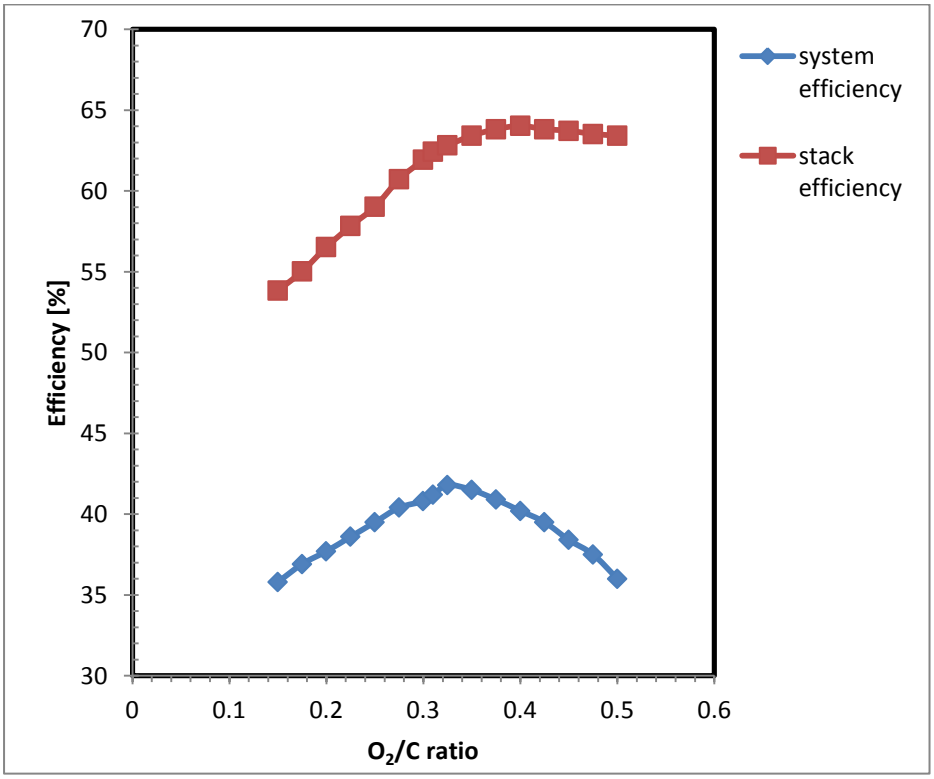

Figure 11: Effect of Varying in O2/C Ratio on Performance Metrics

As an increase in O_2/C ratio is observed, the mass flow rate of air into the system increases. Additional air enters the auto-thermal reformer, which then initially increases the hydrogen production in the reformer and lowers the fuel feed requirements for the stack.

It can also been seen from Figure 11, that above a value of O_2/C ratio of 0.32 (approximately), the system efficiency decreases. This is the result of excess oxygen in the reformer along consuming hydrogen and leading to complete combustion to H_2O and CO.

The increase in the O_2/C ratio value also causes a decrease in system exhaust temperature. This is due to the increased heating requirement for the additional air feed.

3.5.2 Effect of Varying S / C ratio:

The molar flow rate of water entering the system was determined by the S to C ratio and the diesel fuel feed rate. Figure 12 shows the change in net system and stack efficiencies with the increasing S to C ratio.

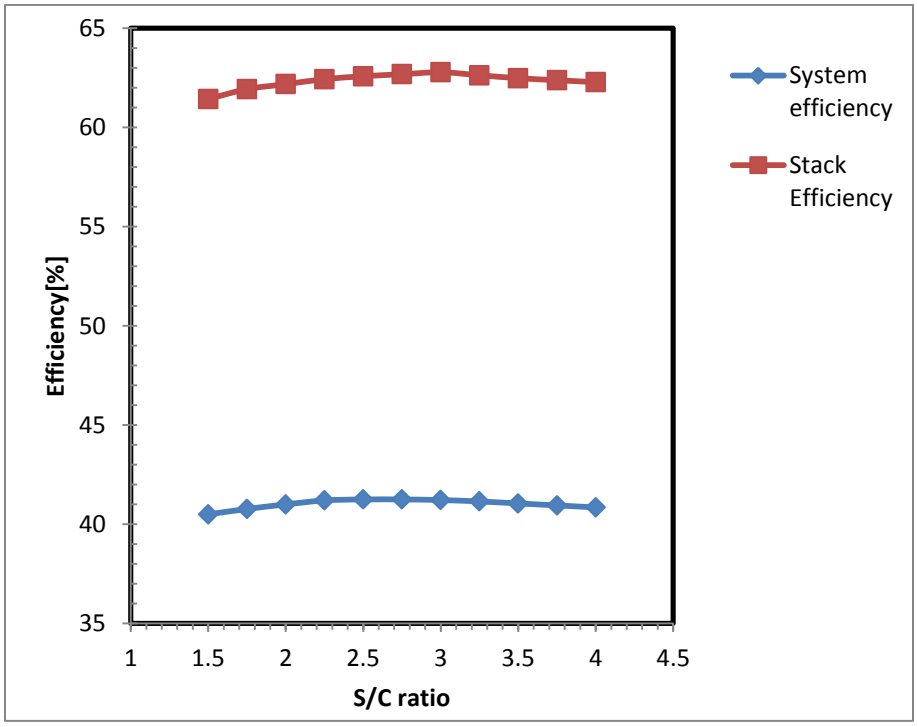

Figure 12: Effect of S/C ratio on Performance Metrics

Figure 12 shows that an increase in the S to C ratio led to a slight rise in the net system and stack efficiency, as the hydrogen yield in the ATR increased. For S/C ratio higher than 2.0, as more steam was added, the H_2 flow in the stack became increasingly diluted resulting in lower partial pressure of hydrogen and consequently lower stack power output and lower overall efficiency [4].

Operating the system with an S/C ratio of below 2, however, is not desirable, due to the possibility of carbon formation in the reformer and the stack [1]. It was also observed during simulations that with the increase in S/C ratio value, the system exhaust temperature decreases due to the added heating requirements.

It should be noted that this analysis has focused on as the performance metrics of system and fuel cell stack efficiency. To obtain a better understanding of the system performance, more than two design variable variations, such as changing the cathode temperature, should be analyzed.

Works Cited

[1] Dhingra. H, P. B. (2013). Sensitivity analysis of a 1kW diesel fuelled SOFC generator. *Journal of Power Sources*, 1-11.

[2]Costamagna, P. (2004). *Chemical Engineering Journal, 102*, 61-69.

[3]Hoogers, G. (2003). *Fuel Cell Technology HandBook.* CRC Press.

[4]Kang I. (2008). *International Journal of Journal Enegy*, 6298-6307.

[5] Kee, R. J., Zhu, H., & Goodwin, D. G. (2004, July 29). Solid-oxide fuel cells (SOFC) with hydrocarbon and hydrocarbon-derived fuels. Golden, Colorado, United States of America

[6]Rostrup-Nielsen JR, C. L. (2011). Concepts in Syngas Preparation. London:

Imperial College.

[7]Rostrup-Nielsen, J. (2002). Large Scale Hydrogen Production. 150 – 159

[8]Qi A, W. S. (2005). Autothermal Reforming of n-octance on Ru-based catalysts, Applied Catalysis.

71-82.

[9]Fontell E, K. T. (2004). Conceptual study of a 250kW planar SOFC system for CHP application. Power Sources, 49-56

[10]Rostrup-Nielsen J.R. (2011). Steam Reforming in Fuel Cells. In D. Shekhawat, Fuel Cells: Technologies for Fuel Processing (pp. 63-65). Amsterdam.

[11] Shekhawat, D. (2011). Introduction to Fuel Processing. Amsterdam: Elisvere

Chapter 4

Modelling and Charecterization of a Tail-Gas Burner

4.1 Model Description:

In this chapter, analysis of a tail-gas burner, used for a 1kW SOFC diesel fuelled system at steady-state conditions is presented. The model is based on a tail-gas burner design used at NRC-IFCI for a 1kW syngas SOFC system [1]. COMSOL™ was used to develop the computational model. Figure 13 shows the original design of the tail-gas burner developed at NRC-IFCI. Further details explaining the setup of the tail-gas burner are given below.

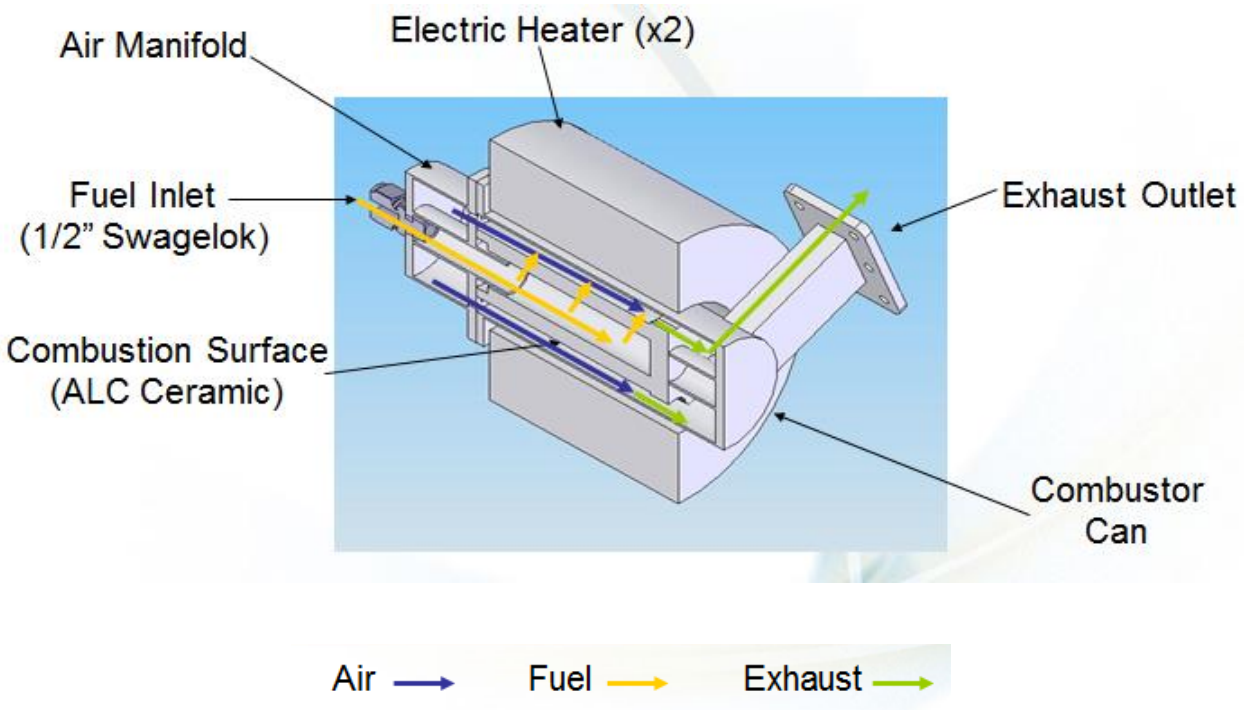

Figure 13: Original design of the tail-gas burner [1]

Anode exhaust from the 1kW diesel-fuelled SOFC system is used as the fuel for the tail-gas burner. Cathode exhaust is used as the air feed to the burner. The burner uses a porous ceramic media to support

the combustion of excess fuel. A non-premixed feed, as opposed to the more commonly utilized premixed feed, was modeled as per the NRC-IFCI design. It should be noted that there has been very limited research published on non-premixed combustion in porous ceramic burners.

The majority of the operating conditions are based on information provided by NRC-IFCI personnel. For the purpose of modelling the incoming fuel was preheated to the 800 -900K around the porous region [1]. The fuel permeates through the porous media and reacts with oxygen from the air inlet on the outer ceramic surface. The hot product gas and any unreacted fuel and air are released into the atmosphere after passing through a series of heat exchangers that are used to preheat incoming fuel, air and possibly steam in some system configurations.

Porous media combustion offers high power density, high power dynamic range and very low NO and CO emissions. This is due to high level of conductivity, emissivity and heat capacity of the solid porous matrix. Radiation and conduction helps in the distribution of the heat produced in the high temperature reaction zone to pre-heat porous solid in the preheat zone. According to Adam Tuck's design (Figure 1), the preheat zone and combustion can is surrounded by electric heaters for startup and to maintain temperature during transients [1].

For the given design, when the system is started, the electric heater is also switched on to ensure temperature stability in the combustor can of the tail-gas burner. As combustion takes place in the burner, the electric heater switches off and the temperature of the can is held constant, due to the heat released by combustion reactions.

In order to make the model more symmetrical, some changes were made to the geometry of the burner while replicating it in COMSOL™. Figure 14 show the geometry of the burner in COMSOL™.

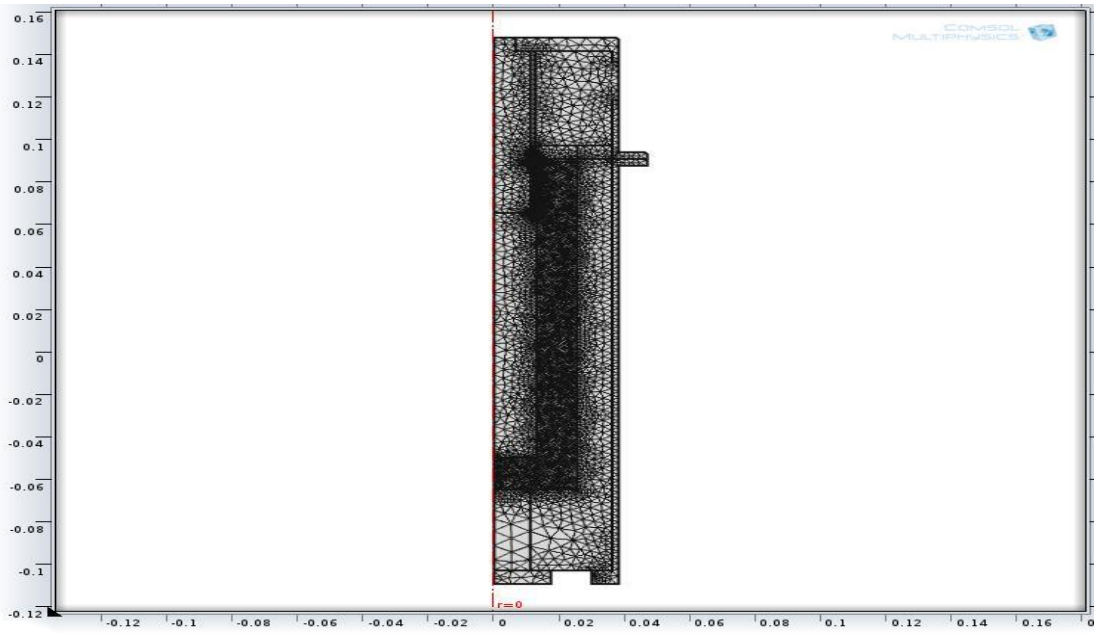

Figure 14: Initial Geometry of the Afterburner in COMSOL (all dimensions are in meters)

Anode and cathode exhaust enter from the air inlet region, marked in figure 13 (Air manifold in figure 13). The gases permeate through the porous media and reacts on the outer boundary of the porous media zone, also defined as the combustion surface in figure 13. In this system, a non-premixed gas flow system is employed with gas being mixed and reacted in the porous media zone. This analysis is compared in detail with pre-mixed feed to the burner in later sections.

4.1.1 Assumptions

The fuel compositions of the anode and cathode exhausts are taken from the VMGSim™ model developed and discussed in the previous chapter. The following tables list the initial mole fraction of the components in the fuel and air inlet feeds

- Fuel inlet equilibrium mole fraction:

Table 6: Mole Fraction of the Gases in the Fuel Inlet

Component	Fraction
Hydrogen – H_2	0.09954
Nitrogen – N_2	0.15972
Water Vapor –H_2O	0.56183
Methane – CH_4	0.00077
Carbon Monoxide –CO	0.04033
Carbon Dioxide – CO_2	0.13776

- Depleted Air inlet mole fraction:

Table 7: Mole Fraction of the Gases in the Air Inlet

Component	Fraction
Oxygen – O_2	0.16538
Nitrogen – N_2	0.83462

Some of the assumptions made while designing the system are given below:

1. The thermo-physical properties of the air (density, thermal conductivity and specific heat) are set to be functions of the temperature and species concentration.
2. The pressure drop through the porous burner is not high; hence, its effect on the thermo-physical properties has been neglected.
3. The properties of the solid phase material are set as constant.
4. There is thermal non-equilibrium between the gas and the solid phase material.

5. The property of the porous material is assumed homogeneous and does not get affected by changing temperature.
6. N_2 was assumed inert during all combustion reactions in the tail-gas burner
7. Materials used to develop the tail-gas burner [1]:
    - 410S Stainless Steel
    - 316SS Swagelok Fittings (1/2" Fuel and 1" Air)
    - Zircar Porous Alumina Tube (Type ALC, density ~18lb/ft^3)
    - Alumina/Silica Rope seal
    - Mica Gaskets
    - Integrated Electric Preheater - Watlow VS403J06S (450Wx2)
8. The basic equation governing the combustion of gaseous fuels in porous media and the resulting heat transfer modes are energy, continuity and species conservation equations.
9. In COMSOL™, these governing equations are defined by built-in equation interfaces such as: reaction engineering interface; compressible navier stokes interface (fluid flow module), conduction and convection interface (heat transfer module); diffusion and convection interface (mass transfer module).

4.1.2 Boundary Conditions:

The boundary conditions, for each section of the tail-gas burner, are given in tables below.

Fluid Flow module:

Table 8: Boundary Conditions for fluid flow module

Section of the burner	Boundary Conditions	Equations
Outer Boundaries	No Slip	$u = 0$

Air Inlet	Laminar Inflow	$L_{entr}\nabla_t \times pI = -np_{entr}$ *where pentr = inlet pressure*
Fuel Inlet	Laminar Inflow	$L_{entr}\nabla_t \times pI = -np_{entr}$
Inlet walls	Walls, no slip	$u = 0$
Porous media	Continuity	$\underline{n}(\eta_i(\nabla u_i + (\nabla u_i)^T) - \left({}^{2\eta_i}/_{3} - \kappa_{dv,i}\right)(\nabla u_i)I - p_i I = 0$
Exhaust outlet	Pressure, no viscous stress	$\underline{n}[(\eta(\nabla u + (\nabla u)^T) - \left({}^{2\eta}/_{3} - k_{dv}\right)(\nabla u)I] = 0$ *where p=po*

Heat Transfer module:

Table 9: Boundary Conditions for heat transfer module

Section of the burner	Boundary Conditions	Equations
Outer Boundaries	Convection Flux	$\underline{n} \times (-D\nabla T) = 0$ *where* $\underline{n}$ *is outward geometry normal*
Air Inlet	Temperature	$T = To$
Fuel Inlet	Temperature	$T = To$
Inlet walls	Continuity	$\underline{n} \times (q_1 - q_2) = 0$ *where* $q_i = -k\nabla T_i$
Porous media	Continuity	$\underline{n} \times (q_1 - q_2) = 0$ *where* $q_i = -k\nabla T_i$
Exhaust outlet	Convective Flux	$\underline{n} \times (-D\nabla T) = 0$

Mass Transfer Module:

Table 10: Boundary Conditions for mass transfer module

Section of the burner	Boundary Conditions	Equations
Outer Boundaries	Convection Flux	$\underline{n} \times (-D\nabla c) = 0$ *where* $\underline{n}$ *is outward geometry normal*
Air Inlet	Concentration	$C = Co$
Fuel Inlet	Concentration	$C = Co$
Inlet walls	Continuity	$\underline{n} \times (N_1 - N_2) = 0$ *where* $N_i = -D_i\nabla c_i + c_i u_i$

Porous media	Continuity	$\underline{n} \times (N_1 - N_2) = 0 \; where \, N_i = \; -D_i \nabla c_i + c_i u_i$
Exhaust outlet	Convective Flux	$\underline{n} \times (-D \nabla c) = 0$

4.1.3 Governing Equations:

The energy equation for the gas phase combustion modelling is given below [3]:

$$\frac{\partial}{\partial t}\left(\varphi \rho_g C_{pg} T_g\right) + \frac{\partial}{\partial x}\left(\varphi \rho_g C_{pg} u T_g\right) = \frac{\partial}{\partial x}\left(\varphi k_g \frac{\partial T_g}{\partial x}\right) - \; (1 - \emptyset) h_v \left(T_g - T_s\right) + \varphi \Delta H_c S_{fg} \quad \text{(Equation 10)}$$

The energy equation for the solid phase used for combustion modelling is [3]:

$$\frac{\partial}{\partial t}(\rho_s C_s T_s) = \frac{\partial}{\partial x}\left(k_s \frac{\partial T_s}{\partial x}\right) - h_v \left(T_s - T_g\right) - \nabla * F \quad \text{(Equation 11)}$$

The "∇ .F" represents the radiative transport equation and is given by

$$\nabla * F = \; -(1 - \omega)(G - 4E_b) \quad \text{(Equation 12)}$$

G is governed by

$$\nabla^2 G = \; \eta^2 (G - 4E_b) \quad \text{(Equation 13)}$$

and

$$\eta^2 = 3\beta^2 (1 - \omega)(1 - g\omega) \quad \text{(Equation 14)}$$

**subscript g and s refer to gaseous and solid phases, respectively.

The meaning of the symbols used in these equations is shown in the table below:

Table 11: Nomenclature for energy equations [3]

Symbol	Definition	Symbol	Definition
φ	Porosity	ΔH_c	Enthalpy of combustion

ρ	Density	S_{fg}	Rate of fuel consumption per unit volume
C_p	Specific Heat	Ω	Single scattering albedo
T	Temperature	Eb	Planck black body emitted flux
U	Velocity	β	Extinction co-efficient
k	Thermal conductivity	F	Radiative flux
h_v	Volumetric heat transfer co-efficient	g	Asymmetry factor

When these equations are implemented in COMSOL™, the materials and reaction engineering interface is set up with data for most gases provided in CHEMKIN format. These files provide thermodynamic, transport and reaction mechanism data for the reactions of the gases. Hence, most of the data shown in Table 11 is taken and provided in the CHEMKIN files found [7].

The conservation equation for the mass fraction of the fuel is given as follows [3]:

$$\frac{\partial}{\partial t}\left(\rho_g m_E\right) + \frac{\partial}{\partial x}\left(\rho_g u m_f\right) = \frac{\partial}{\partial x}\left(D_{AB}\rho_g \frac{\partial m_f}{\partial x}\right) - S_{fg} \quad \text{(Equation 15)}$$

Where m_f is the fuel mass fraction

The term D_{AB} is the diffusion co-efficient for multi-component mixture and can be defined by [8]:

$$D_{amix} = \frac{1 - x_a}{\left(\frac{x_b}{D_{ab}}\right) + \left(\frac{x_c}{D_{ac}}\right) + \left(\frac{x_d}{D_{ad}}\right) + \ldots} \quad \text{(Equation 16)}$$

Where

xa = mole fraction of component “a”.

Dab = Binary Diffusion coefficient of component “a”, diffusing through component “b”, in m2/sec.

Damix = Diffusion coefficient of component “a”, relative to gas mixture, in m2/sec.

The Binary Diffusion coefficient is defined by the following equation [6]:

$$D_{ab} = 1.883e-22\left(\frac{T^{3/2}}{P\sigma_{ab}\Omega_D}\right)\sqrt{\frac{M_a + M_b}{M_a M_b}} \quad \text{(Equation 17)}$$

This is an empirical equation to calculate the value of the diffusion coefficient.

Where

σ_{ab} = Lennard-Jones characteristic length of the mixture, in m.

Ω_D = Dimensionless collision integral for diffusion

P = Pressure in Pa.

T = Temperature in K.

Ma = Molecular weight of component "a", in kg/mol.

The Lennard-Jones characteristic length can be calculated using the following equation [6]:

$$\sigma_{ab} = \frac{1}{2}\left(\sigma_a + \sigma_b\right) \quad \text{(Equation 18)}$$

And [6]:

$$\Omega_D = \frac{1.06036}{\left(T^*\right)^{0.15}} + \frac{0.193}{\exp\left(0.47635T^*\right)} + \frac{1.03587}{\exp\left(1.52996T^*\right)} + \frac{1.76474}{\exp\left(3.89411T^*\right)} \quad \text{(Equation 19)}$$

The collision integral for diffusion (ΩD) is a function of the dimensionless temperature:

$$T^* = \left(\frac{k}{\varepsilon_{ab}}\right)T$$

Where:

k = Boltzmann constant

εab = characteristic mixture energy parameter

The mixture energy parameter ε_{ab} can be estimated in terms of the Lennard-Jones 12-6 potential characteristic energies for species "a" and "b" (ε_a and ε_b) according to [6]:

$$\varepsilon_{ab} = \sqrt{\varepsilon_a \varepsilon_b} \quad \text{(Equation 20)}$$

Other than the equations below, some of other equations used to calculate values for multi-component mixtures are given below:

Molar flow rate:

$$M_{inlet} = x_{H_2} M_{H_2} + x_{CO} M_{CO} + x_{CO_2} M_{CO_2} + ... \quad \text{(Equation 21)}$$

Density:

$$\rho_{inlet} = \frac{M_{inlet} P}{RT} = \frac{\left(x_{H_2} M_{H_2} + x_{CO} M_{CO} + x_{CO_2} M_{CO_2} + ..\right) P}{R\,T} \quad \text{(Equation 22)}$$

$$\rho_{porous} = \frac{M_{porous} P}{RT} = \frac{\left(x_{inlet} M_{inlet} + x_{H_2O} M_{H_2O} + x_{O_2} M_{O_2} + ...\right) P}{R\,T} \quad \text{(Equation 23)}$$

The viscosity equation with diffusion co-efficient and density parameters:

$$\mu_{mix} = \sum_{i=1}^{n} \frac{\mu_i}{1 + \left[\frac{1.385 \mu_i}{x_i \rho_i} \sum_{\substack{j=1 \\ i \neq j}}^{j=n} \frac{x_i}{D_{ij}} \right]} \quad \text{(Equation 24)}$$

Simplifying the viscosity equation:

$$\mu_{mix} = \sum_{i=1}^{n} \frac{\mu_i}{1 + \frac{1}{x_i} \sum_{\substack{j=1 \\ j \neq n}}^{n} \frac{x_j \left[1 + \left(\mu_i / \mu_j \right)^{1/2} \left(M_j / M_i \right)^{1/4} \right]^2}{2\sqrt{2} \left[1 + \left(M_i / M_j \right) \right]^{\frac{1}{2}}}} \quad \text{(Equation 25)}$$

4.1.4 Reaction Kinetics:

The reaction mechanism and kinetics for the combustion modelling of the anode exhaust are similar to the combustion of methane, as the species utilized in the anode exhaust and methane combustion are the same (H_2, CH_4, N_2, O_2, CO, CO_2, H_2O). The detailed reaction mechanism of methane and hydrogen combustion contains 53 species, also known as GRIMECH 3.0 [7]. COMSOL™ does not provide flexibility for more than 20 species for 2D axisymmetric modelling; hence, a reduced combustion model was implemented for the purposes of this study.

At this time, there are many different chemical schemes available. These can be seen in the table below.

Table 12: Chemical schemes available for gas species involved in this study [4]

Fuel/oxidizer	Scheme name	Number of Species	Number of reactions
CH_4/air	GRI Mech 3.0	52	323
CH_4/air	2S-CM2	5	2
CH_4/air	J-L(Jones-Linstedt)	6	4
$CH_4/O_2/CO_2$	GRI Mech 3.0	34	215
$CH_4/O_2/CO_2$	2S-CM2	5	2
$CH_4/O_2/CO_2$	J-L(Jones-Linstedt)	7	6

Since it is a multi-component feed with methane involved, the reaction engineering module was used to simplify the set-up of reaction equations and thermodynamic factors in addition to the transport properties.

A comparison of the reaction kinetics models was done between a detailed conventional methane combustion model (GRI Mech 3.0 -53 species and 323 equations) and a more simplified version (J-L method- 7 species and 6 equations). 0D reaction engineering module in COMSOL™ is used for the comparison of these models. Similar inlet conditions were applied to the reaction engineering module for both mechanisms. This was done to verify whether the reduced combustion model could be used instead of the detailed model, as the latter had compatibility problems with 2D modelling in COMSOL™.

Figure 15 shows the comparison of the temperature profiles between GRIMECH 3.0 and the 6-step mechanism model.

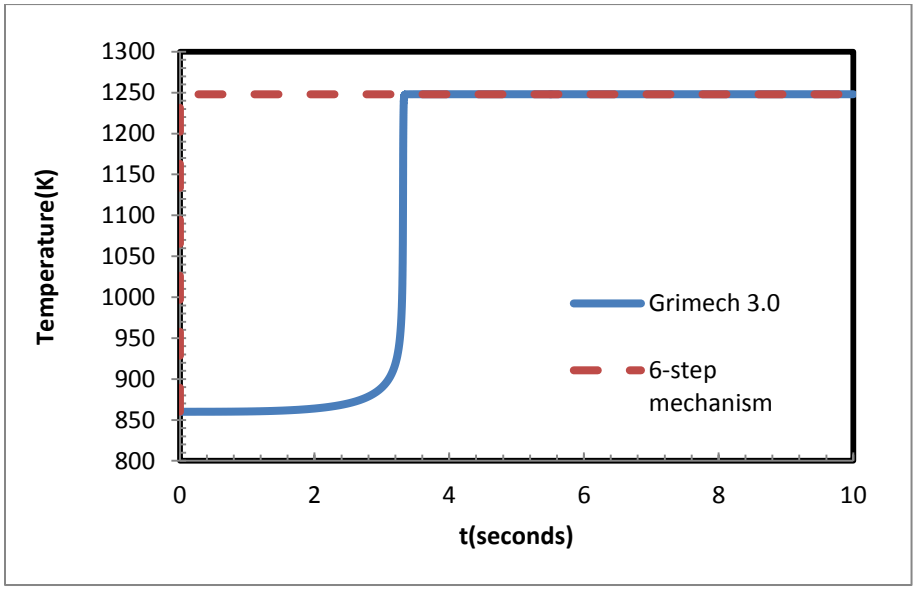

Figure 15: Comparison of Temperature profile for the Two Mechanisms

Figure 16 compares the H_2 and CH_4 concentration of these two mechanisms

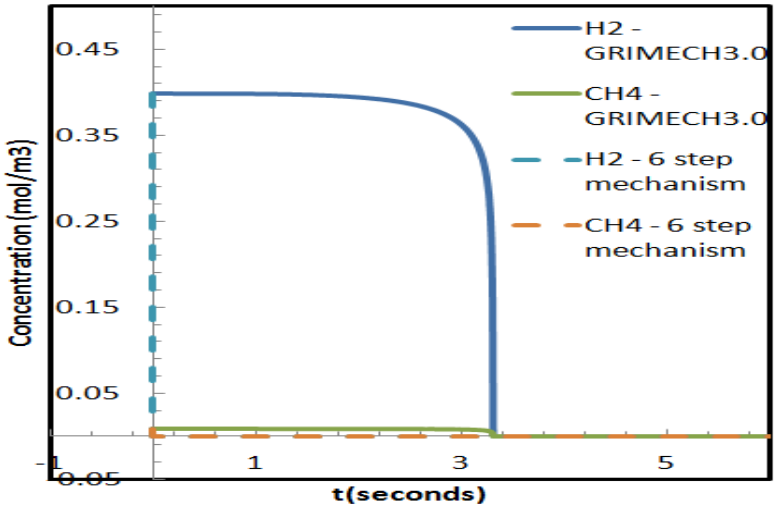

Figure 16: H2 and CH4 Concentration comparison of the Two Mechanisms

This comparison shows that using the 6-step mechanism (J-L scheme) will provide similar results to the GRIMECH 3.0 mechanism. The 6-step mechanism is now used in the reaction engineering module, which is coupled with the 2D –axisymmetric model used in the hydrogen combustion.

The reduced combustion mechanism used for the analysis of the anode exhaust from the 1kW fuel cell can be seen below:

Table 13: Reaction Mechanism for the anode exhaust fuel stream [4]

Reaction number	Reaction	Pre-exponential Factor (A)	Activation Energy (Ea)
1	$CH_4 + 0.5O_2 \rightarrow CO + 2H_2$	$3.5 \times 10^9\ m^{1.5}\ mol^{-0.5}\ s^{-1}$	125520 J/mol
2	$CH_4 + H_2O \rightarrow CO + 3H_2$	$3 \times 10^8\ m^3\ mol^{-1}\ s^{-1}$	125520 J/mol
3	$H_2 + 0.5O_2 \rightarrow H_2O$	$3.5 \times 10^{14}\ m^{1.5}\ mol^{-0.5}\ s^{-1}$	167360 J/mol
4	$CO + H_2O \leftrightarrows CO_2 + H_2$	$2.75 \times 10^9\ m^3\ mol^{-1}\ s^{-1}$	83680 J/mol
5	$CH_4 + 1.5O_2 \rightarrow CO + 2H_2O$	$2 \times 10^6\ m^{4.5}\ mol^{-1.5}\ s^{-1}$	146440 J/mol
6	$CO + 0.5O_2 \rightarrow CO_2$	$2 \times 10^6\ m^{1.5}\ mol^{-0.5}\ s^{-1}$	50208 J/mol

4.2 Design Analysis:

Using the initial CAD design provided by NRC-IFCI [1], a COMSOL™ model was developed with a few modifications to the original design to simplify the modelling. The air domain was divided in two sections and the reaction zone was defined as the outer boundary of the porous media domain, formerly shown as the combustion surface in Figure 13. The outer boundary of the porous media domain is set as the reaction zone, as the fuel and air feed combine and would combust on that surface, due to high temperature of inlet feeds. Electric heater was also added to the geometry, which is used initially used to heat the inlet feeds and during the later stages of combustion, as insulation. The following figure shows a detailed inner flow path through the tail-gas burner.

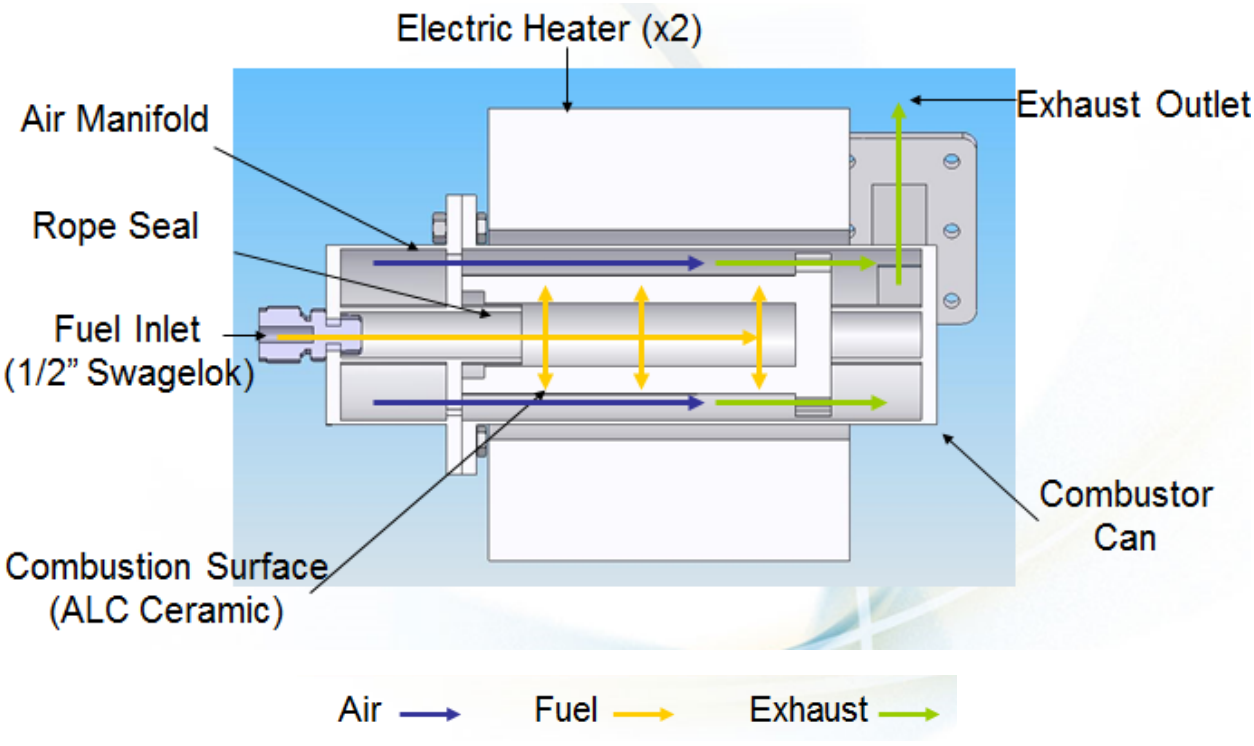

Figure 17: Detailed inner flow design of the burner [1]

The following table lists the baseline input values chosen for the runs in the model. These values are based on discussions with Adam Tuck of NRC-IFCI, the system model described in Chapter 3, information from the literature and manufacturers specifications for specific materials.

Table 14: Baseline Parameters for Anode Exhaust Tail-gas Burner Model

Parameters	Values
Porosity	0.93**
Permeability	1e-9[m^2]**
Outlet Pressure	101,325 [Pa]
Fuel Inlet Temperature	860[K]
Air Inlet Temperature	800[K]
Volumetric flow rate of fuel inlet	7.135[m^3/hr]
Volumetric flow rate of air inlet	24.112[m^3/hr]
Hotbox Temperature	700[K]
Thermal Conductivity of Porous material (k_p)	0.19 [W/m.K]**
Density of the Porous material (ρ_p)	240 [kg/m^3]**
Heat Capacity of Porous material ($C_{p.p}$)	1047[J/kg.K]**

** Zircar Ceramic porous media used [9]

4.2.1 Base Case Performance:

Figure 18 shows the new geometry design developed in COMSOL™.

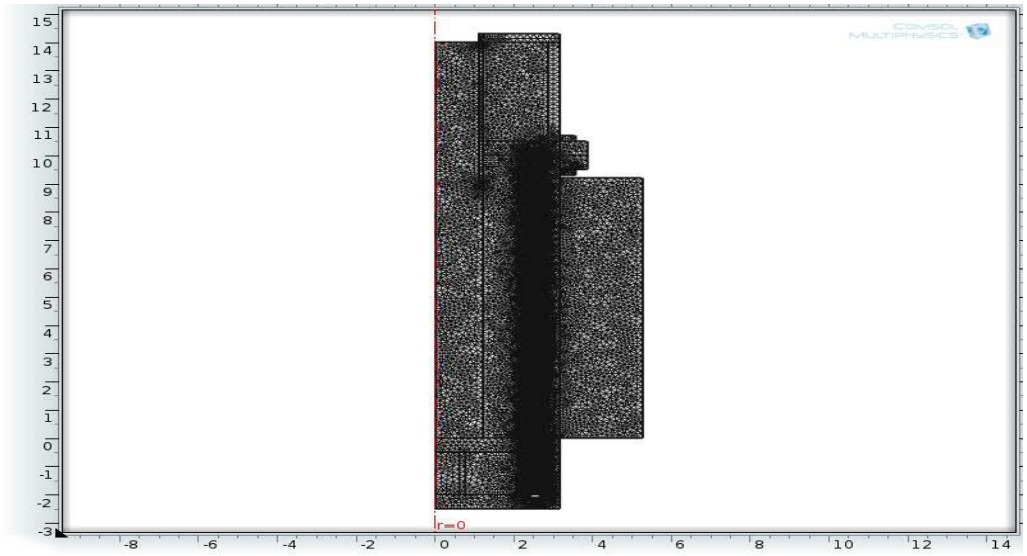

Figure 18: New Geometry for the Afterburner model (all dimension in centimeters)

The region where the mesh is highly refined, as shown in Figure 18, is defined as the reaction zone for this model.

The fuel flow enters the fuel chamber and permeates through the porous media region to the outer surface where the fuel reacts with the air entering from the air manifold. The product gas flows through the exhaust outlet. Heat produced by the combustion reaction is used to heat the inlet fuel and air and is used elsewhere in the 1kW diesel fuelled SOFC system.

Fluid flow interface, heat transfer and mass transfer interfaces are applied to the burner in COMSOL™. For the analysis of the burner; velocity, temperature and concentration profiles across the burner are evaluated. All results are for steady-state operation.

Velocity Profile:

The average operating temperature was maintained around 593ºC and the fuel inlet velocity was set to 7 m/s, air inlet velocity was set at 19 m/s. The flow was modelled using the following equations.

Flow in the open channel was modelled using the Navier-Stokes equations:

$$\boldsymbol{\rho}\frac{\boldsymbol{\partial u}}{\boldsymbol{\partial t}} + \boldsymbol{\nabla} * \left[-\boldsymbol{\eta}\left(\boldsymbol{\nabla u} + (\boldsymbol{\nabla u})^{\boldsymbol{T}}\right) + \boldsymbol{p}\mathbf{I}\right] = -\boldsymbol{\rho}(\boldsymbol{u} * \boldsymbol{\nabla})\boldsymbol{u} \text{ (Equation 26)}$$

Where

$$\nabla * u = 0$$

The Brinkman equation was used to model the flow in the porous media

$$\frac{\boldsymbol{\rho}}{\boldsymbol{\epsilon_p}}\frac{\boldsymbol{\partial u}}{\boldsymbol{\partial t}} + \boldsymbol{\nabla} * \left[-\frac{\boldsymbol{\eta}}{\boldsymbol{\epsilon_p}}\left(\boldsymbol{\nabla u} + (\boldsymbol{\nabla u})^{\boldsymbol{T}}\right) + \boldsymbol{p}\mathbf{I}\right] = -\frac{\boldsymbol{\eta}}{\boldsymbol{k}}\boldsymbol{u} \text{ (Equation 27)}$$

Where

$$\nabla * u = 0$$

Figure 19 shows the shows the results of velocity modelling work

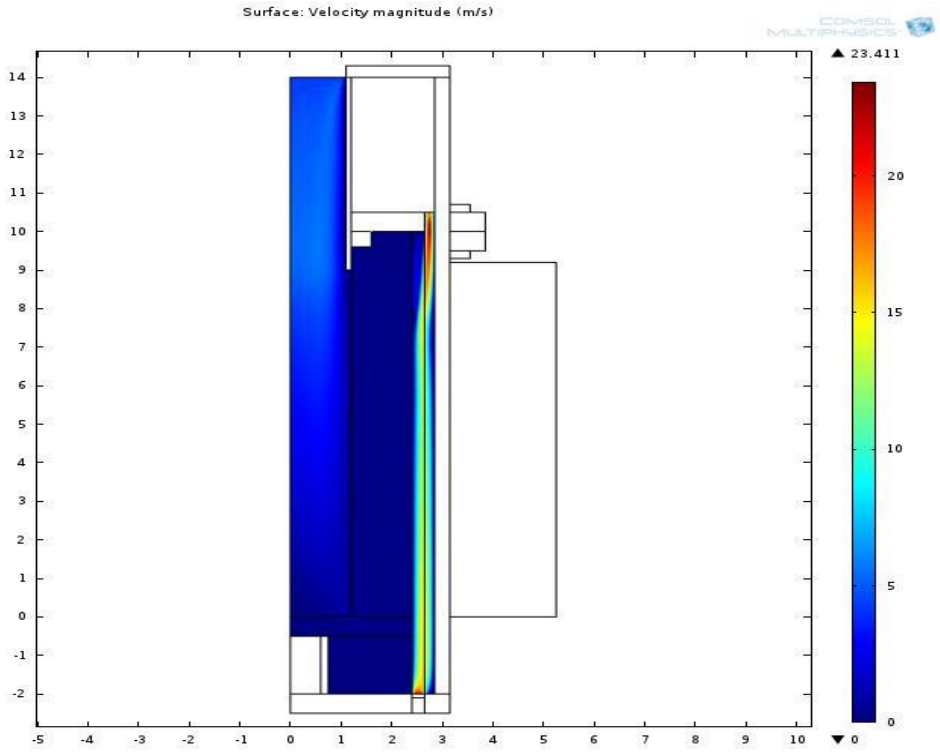

Figure 19: Velocity Distribution in afterburner for above mentioned conditions (Dimensions cm and velocities in m/s)

The inlet velocities were set at 7m/s and 19m/s, to maintain laminar flow conditions in the tail-gas burner. These velocities are consistent with the volumetric flow rate at the entrance of the burner. It can be seen that the velocity of the flow through the porous media is very low. For this scenario, the flow through the porous media, on average, was found to be 0.05m/s.

Temperature Profile:

The temperature of the fuel inlet was set to 860K and the air inlet to 800K. Heat transfer was modelled using the following equations:

Heat transfer in fluids inside the porous media domain, was modelled using the following energy balance equation:

$$\boldsymbol{\rho C_p u} * \boldsymbol{\nabla T} = \boldsymbol{\nabla} * (\boldsymbol{k \nabla T}) + \boldsymbol{Q} + \boldsymbol{W_p} \text{ (Equation 28)}$$

Where

ρ = fluid density

Cp = Heat capacity at constant pressure

u = Horizontal velocity

Q = Quantity of heat

W = Work done

k= Thermal conductivity

Heat transfer through the metal of the burner was modelled using the following equation

$$-\underline{n} * (-\boldsymbol{k \nabla T}) = \boldsymbol{q_0} \text{ (Equation 29)}$$

Where q_o is defined as

$$q_0 = h * (T_{ext} - T)$$

$\underline{n}$ = outward geometry normal

h = convective heat transfer co-efficient of metal

The following figure shows the variation in temperature across the burner.

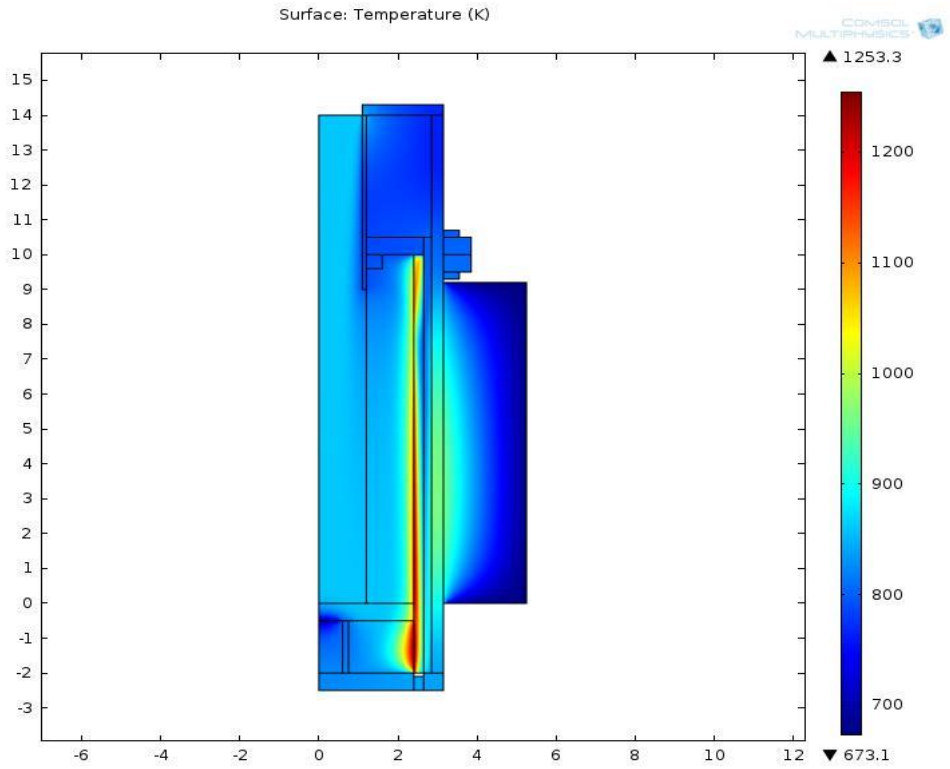

Figure 20: Temperature profile of Anode-exhaust model (all dimensions in centimeters and temperature in Kelvin)

The heat transfer module used to create this profile includes radiant heat transfer within the afterburner as well as heat loss through the metal walls. The distinct local maximum in temperature at the outer boundary of the porous region shows that combustion is limited to that zone. The temperature profile accounts for the diffusion of heat across the materials and chambers in the burner. According to Figure 20, the temperature across the burner seems more stable at around the temperature difference of 20K.

Concentration Profile:

Convection and Diffusion in the burner are defined by the following equations.

$$\nabla * (-D_i \nabla c_i) + u * \nabla c_i = R_i \text{ (Equation 30)}$$

$$N_i = -D_i \nabla c_i + u c_i \text{ (Equation 31)}$$

Figures 21 and 22 indicate the variation in mass fraction across the afterburner for hydrogen, methane and oxygen.

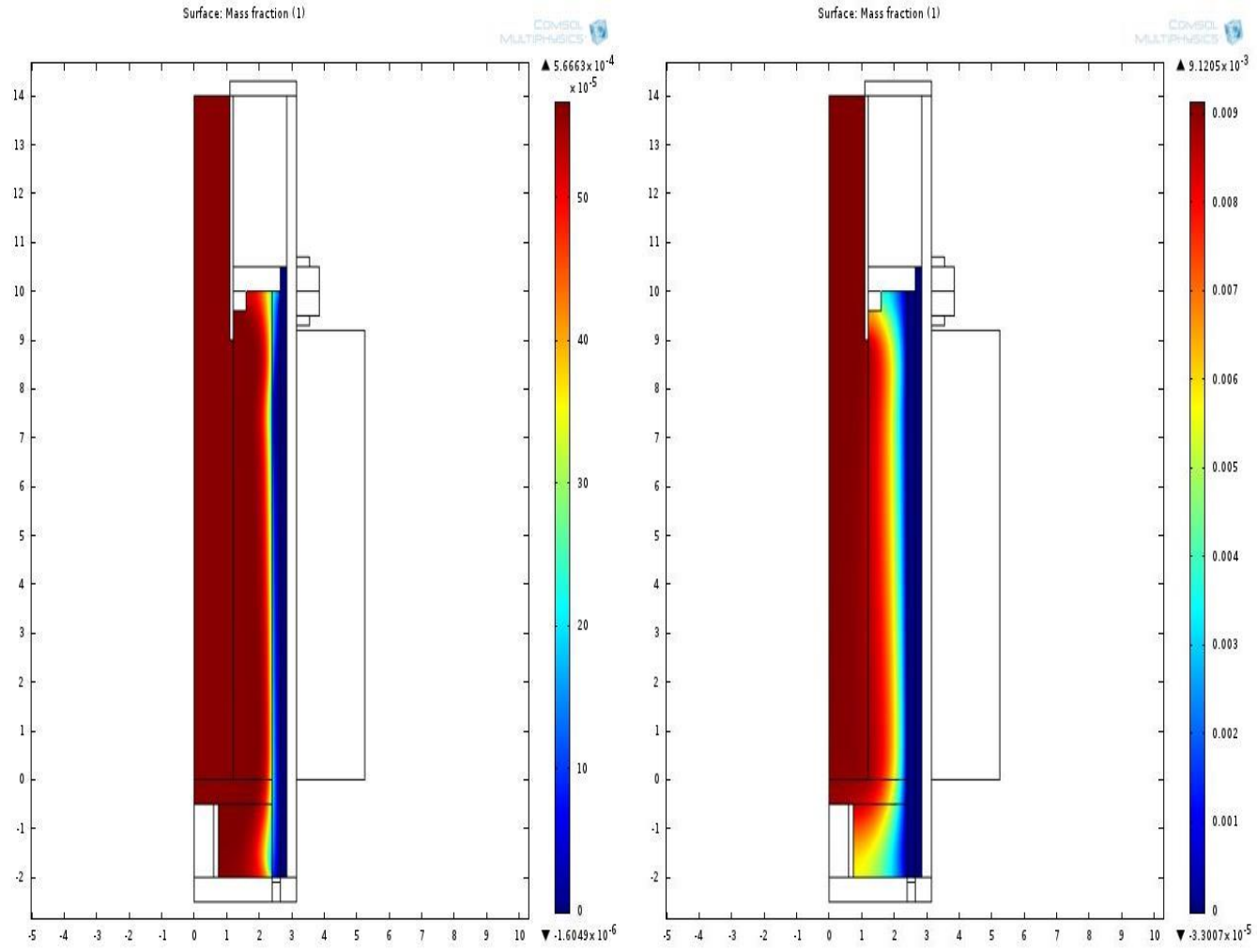

Figure 21: Mass Fraction profiles of Hydrogen and Methane (all dimensions in centimeters)

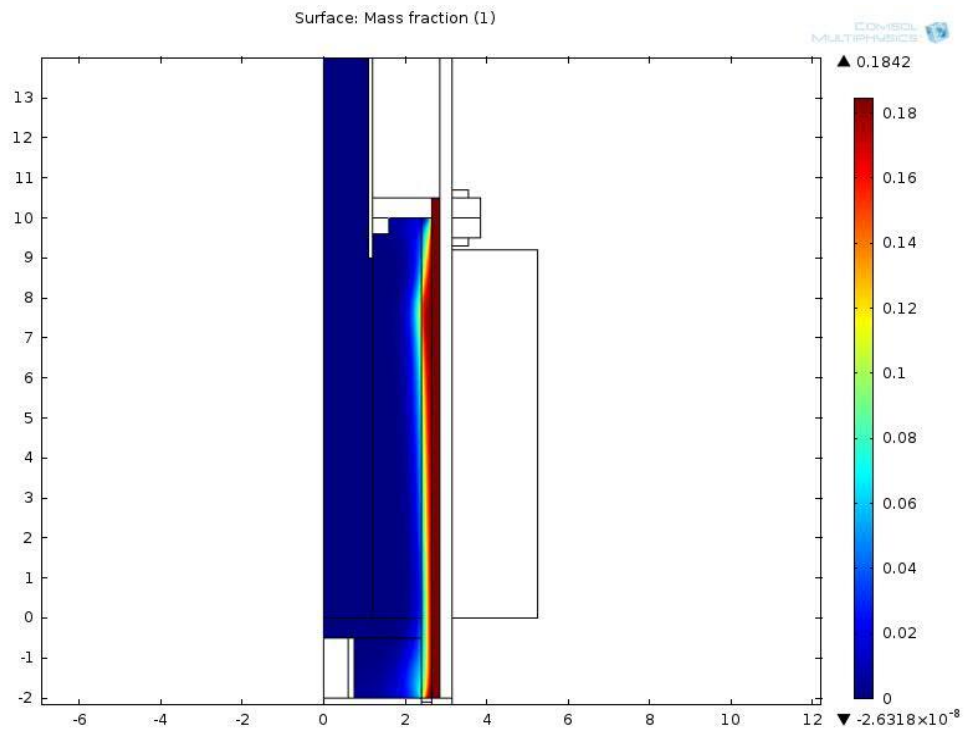

Figure 22: Mass Fraction profile of Oxygen (all dimensions in centimeters)

These profiles show that most of the reactants (hydrogen and methane in particular) are completely used up during the reaction in the after burner. To check the authenticity of the 2D-model, the flow rate of hydrogen in the reaction engineering module is compared to the flow rate of hydrogen in the 2D-model of the afterburner.

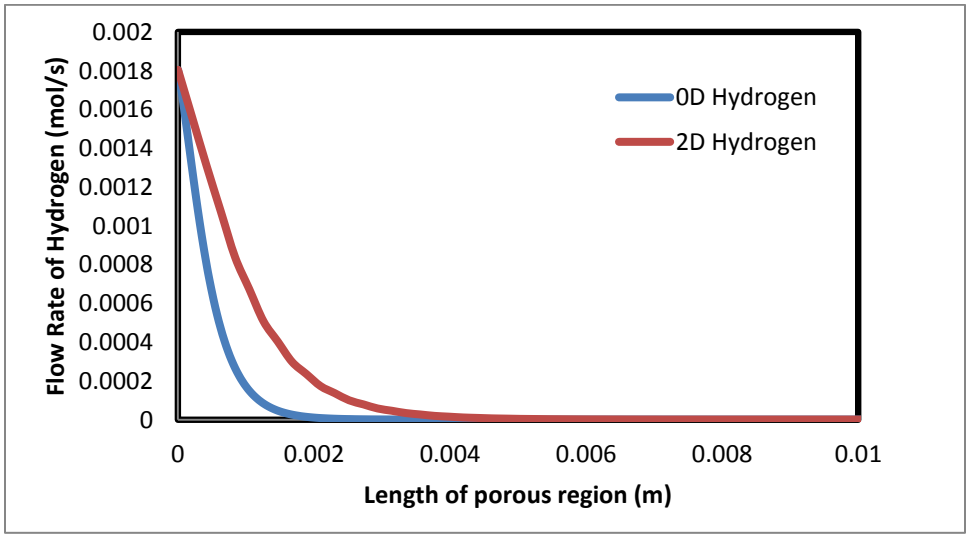

Figure 23: Comparison of flow rates of Hydrogen (all dimension in meters, flow rate in mol/s)

Figure 23 confirms that in both cases, hydrogen is completely consumed during combustion. This confirms that the reaction rate and consumption of the reactants is similar in 0D modelling of the combustion reaction and the 2D-axisymmetric burner model in COMSOL^{TM}.

Figure 24 shows flow rates of all the components across the reaction zone in the afterburner

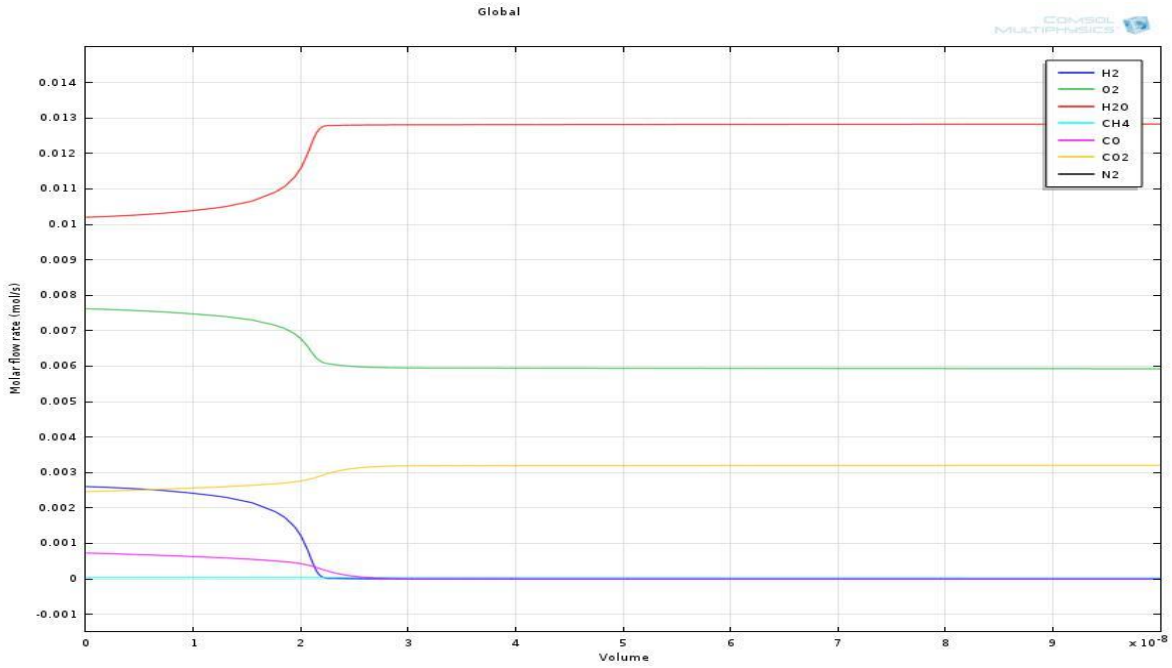

Figure 24: Flow rates of the components across the combustion surface and air/exhaust chamber (all dimension in meters, flow rate in mol/s)

This shows that the concentration of H_2O and CO_2 increases at the exhaust while the molar flow rate of H_2, CH_4 and CO decreases to approximately zero. This also verifies that in the burner, all the unburnt fuel is converted into acceptable exhausts.

To further the understanding of the characteristics of the tail-gas burner, the air and fuel utilization of the SOFC system were varied and the response analyzed. Flows of rich and lean O_2 as well as rich and lean fuel are studied.

4.2.2 Effect of varying air utilization:

Figure 25 shows the change in the outlet temperature with the increasing volumetric flow rate of air with the fuel flow help constant at the baseline value. This represents the situation where the air utilization is decreased in the SOFC stack.

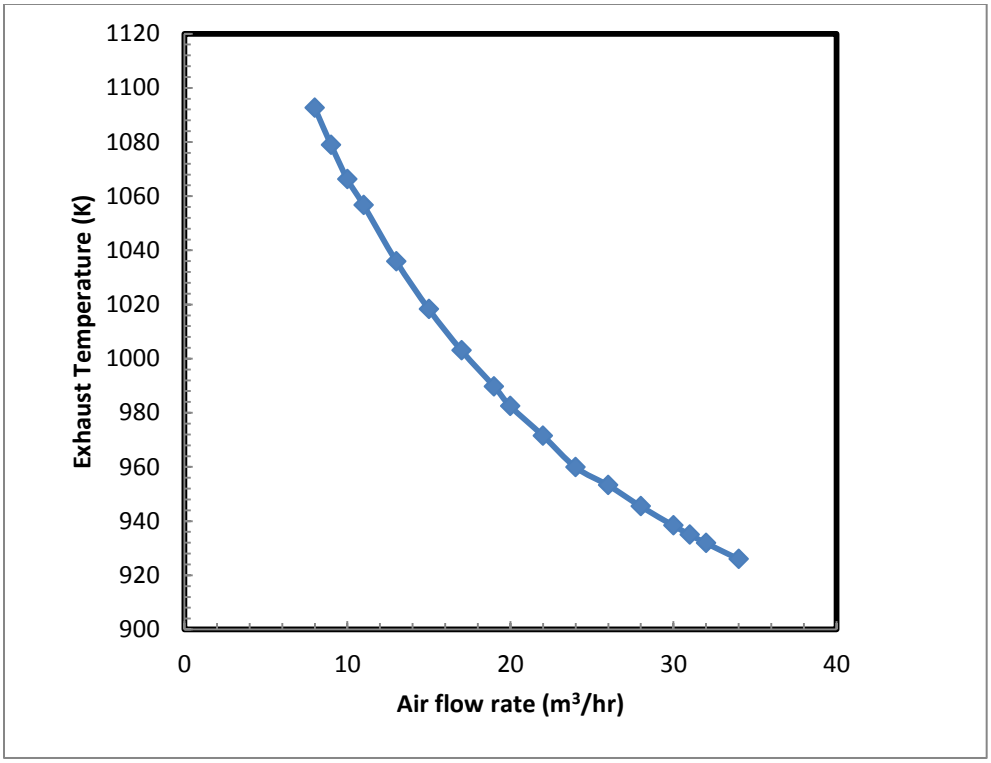

Figure 25: Effect of varying air flow rate on Exhaust Temperature

Figure 25 shows that an increase in the air flow rate (which corresponds to a decrease in air utilization in the SOFC stack) causes a decrease in the outlet exhaust temperature from the burner. When the air utilization of the fuel cell was kept high, the air flow rate to the burner is decreased and the outlet exhaust temperature from the burner is higher than the base case.

When the air utilization of the fuel cell system was decreased, more air is allowed into the system, hence making the mixture in the tail-gas burner rich in O_2. With excess O_2, the outlet temperature decreased and there was a significant amount of nitrogen and unreacted oxygen in the burner exhaust.

4.2.3 Effect of varying fuel utilization:

Figure 26 shows the change in the outlet exhaust temperature of the burner with the increasing volumetric flow rate of fuel.

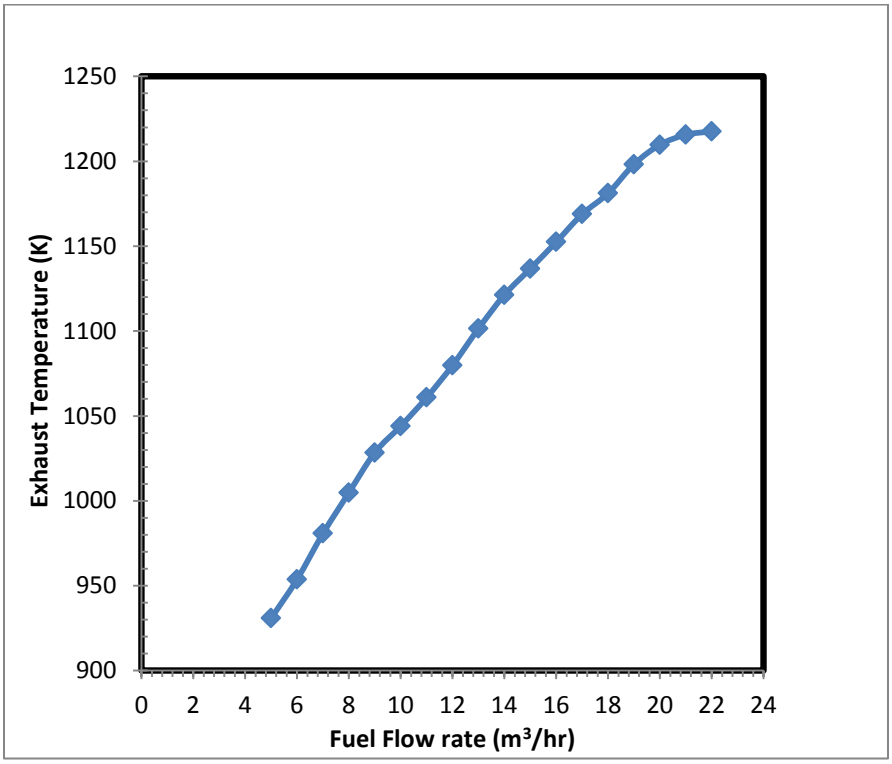

Figure 26: Effect of increasing fuel flow rate on Exhaust Temperature

For this study, the flow rate of air was kept constant for all trials. As shown in Figure 26, an increase in the fuel flow rate (which corresponds to a decrease in fuel utilization) leads to an exponential rise in the burner exhaust temperature.

4.2.4 Premixed Inlet Feed:

The COMSOL™ model was also tested with a premixed inlet feed. Anode exhaust is mixed with the cathode air exhaust and fed into the ceramic tail-gas burner. The study was performed to study the differences in the burner performance and temperature profile compared to the unmixed feed.

Premixed flow enters the burner from the fuel inlet, shown in Figure 18, where the feed is heated around the porous media zone to approximately 850K. The mixture is set to react homogenously on the combustion surface of the ceramic. Table 15 lists the initial mole fractions of the components in the premixed inlet feed.

Table 15: Mole Fraction of the Gases in the Premixed Feed

Component	**Fraction**
Hydrogen – H_2	0.02814
Nitrogen – N_2	0.6439
Water Vapor –H_2O	0.15877
Methane – CH_4	0.00063
Carbon Monoxide –CO	0.0114
Carbon Dioxide – CO_2	0.0383
Oxygen – O_2	0.118

Using a similar set up of the model as before, this analysis was completed. Figure 27 explains the fluid flow of the feed through the burner.

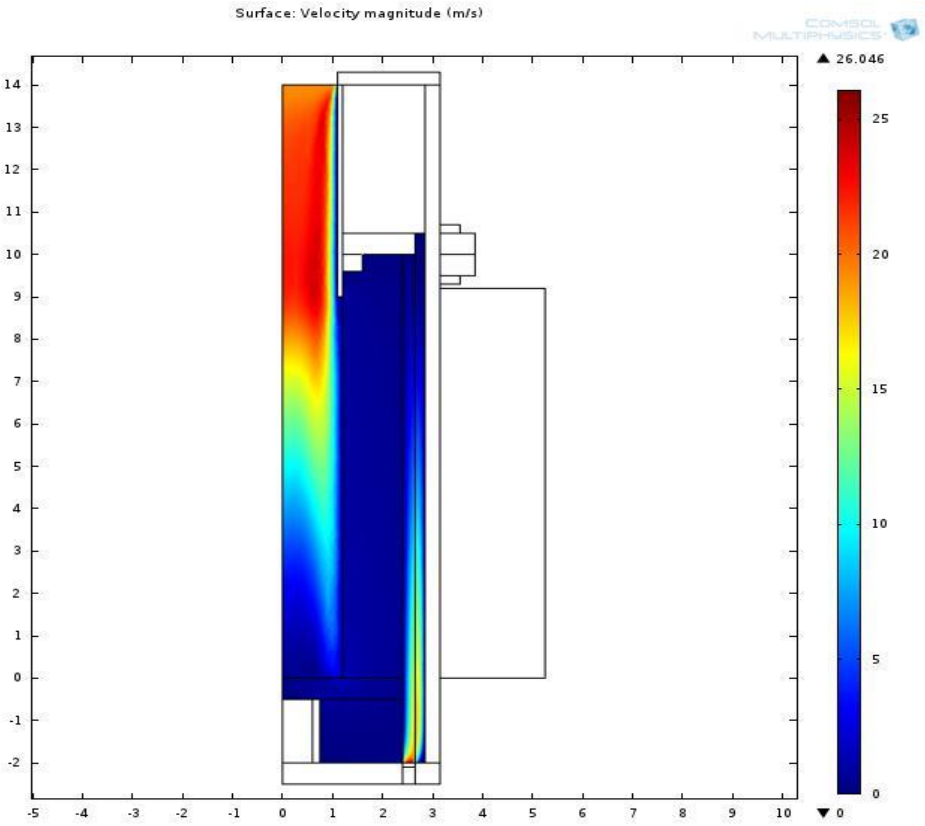

Figure 27: Velocity Profile for premixed feed testing (all dimensions in centimeters, velocity is in m/s)

It can be seen in figure 27 that at the inlet of the feed, the velocity of the flow is at its highest, at approximately 26m/s. The velocity of the flow slows down as it flows through the porous media towards the combustion ceramic surface. The velocity of the flow again increases at the end of the burner due to the opening of the exhaust outlet.

Figure 28 shows the temperature profile for this analysis.

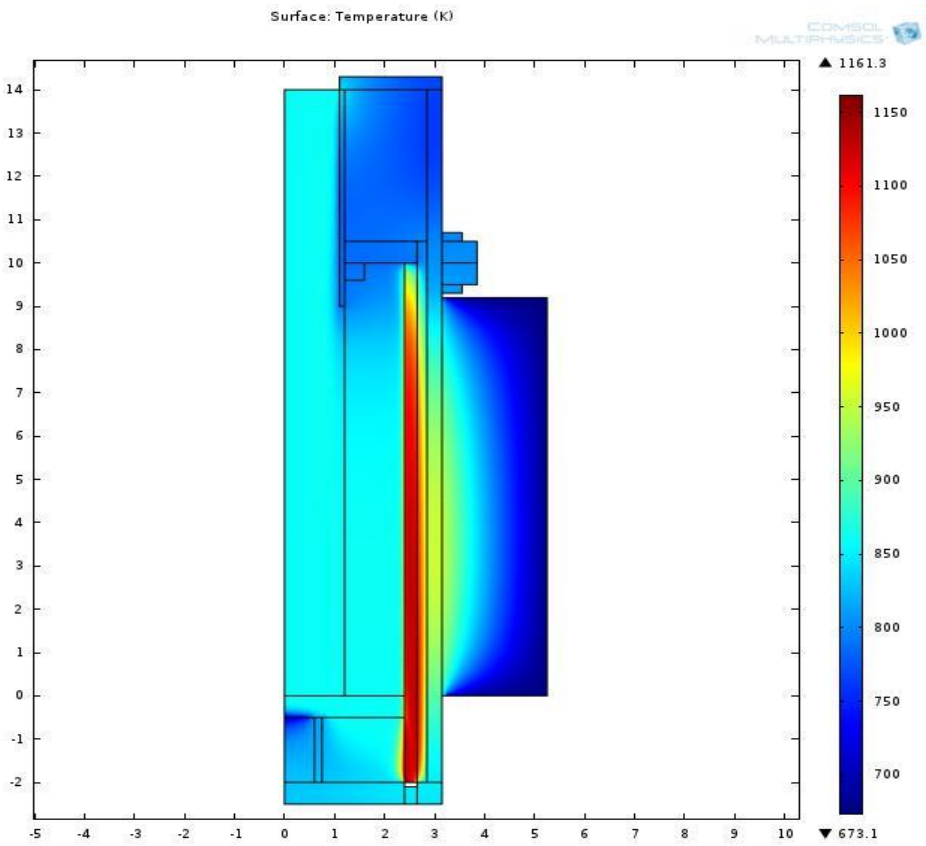

Figure 28: Temperature profile for premixed feed analysis (all dimensions in centimeters, temperature in K)

The temperature profile, shown in figure 28, is very similar to temperature profile shown in figure 20. Heat transfer occurs around the combustion surface as heat is transferred via conduction and radiation to the supporting materials of the burner, and by convection to heat the incoming feed. It is noted that the whole reaction zone is at its highest temperature (red zone in figure 28) in the premixed feed case whereas in the non-premixed feed case, the highest temperature is only found on the combustion surface. This could be attributed to the fact that premixed feed flows through the reaction zone to the air manifold, hence providing better heat distribution along the flow.

Figure 29 shows the hydrogen and methane concentration profile through the burner for premixed feed.

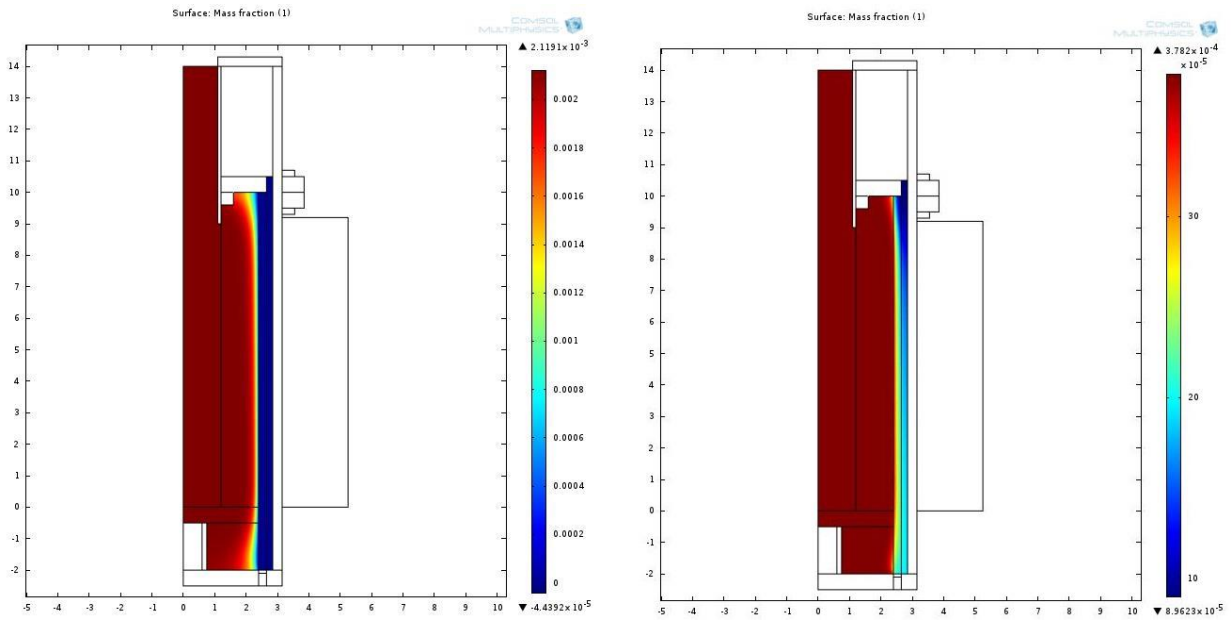

Figure 29: Mass Fraction profiles of Hydrogen and Methane for premixed feed (all dimensions in centimeters)

These profiles are very similar to the concentration profiles in figure 21. The extent of colour change in profiles (decrease in concentration) starts closer to the reaction zone as compared to figure 21. This is due to the decrease in mass fraction of hydrogen and methane due to mixing of the fuel with air. Since, fuel and air are already mixed, the decrease in mass fraction of reactants occurs very close to the combustion zone, due to the reactions.

After viewing the premixed feed results and comparing them to the non-premixed feed, it can be determined that these profiles are similar for both conditions. Table 16 compares the exhaust outlet mass fractions and exhaust temperature for both feeds (premixed and non-premixed).

Table 16: Comparison of exhaust outlet variables for premixed and non-premixed feed

	Premixed Feed	**Non-premixed Feed**
Exhaust Outlet Temperature (K)	1001	959
Component	**Exhaust Mass Fraction**	**Exhaust Mass Fraction**
Hydrogen – H_2	5.2×10^{-6}	1.52e-6
Water Vapor –H_2O	0.13	0.09
Methane – CH_4	2.1×10^{-4}	2×10^{-4}
Carbon Monoxide –CO	2.4×10^{-4}	1.3×10^{-4}
Carbon Dioxide – CO_2	0.08	0.08
Oxygen – O_2	0.12	0.15

Table 16 shows that the outlet temperature and outlet mass fractions for both feed configurations are similar. Based on these criteria it appears that using a non-premixed or premixed feed does not significantly change the performance. Non-premixed feeds, however, may provide more control over the combustion reactions, and the extent of combustion.

4.3 Validation:

The model described above was extended and modified to predict combustion temperatures at outlet exhaust that can be used as a comparison with measured temperatures provided by Adam Tuck of NRC-IFCI for an operating afterburner used in a biogas-fuelled SOFC system. The hotbox, containing the burner, was set at constant temperature of 700K. Air flow rate was initially set constant at $5m^3$/hr, till the fuel flow rate was approximately $7m^3$/hr. Air flow rate was then changed to $15m^3$/hr for the rest of the experiment.

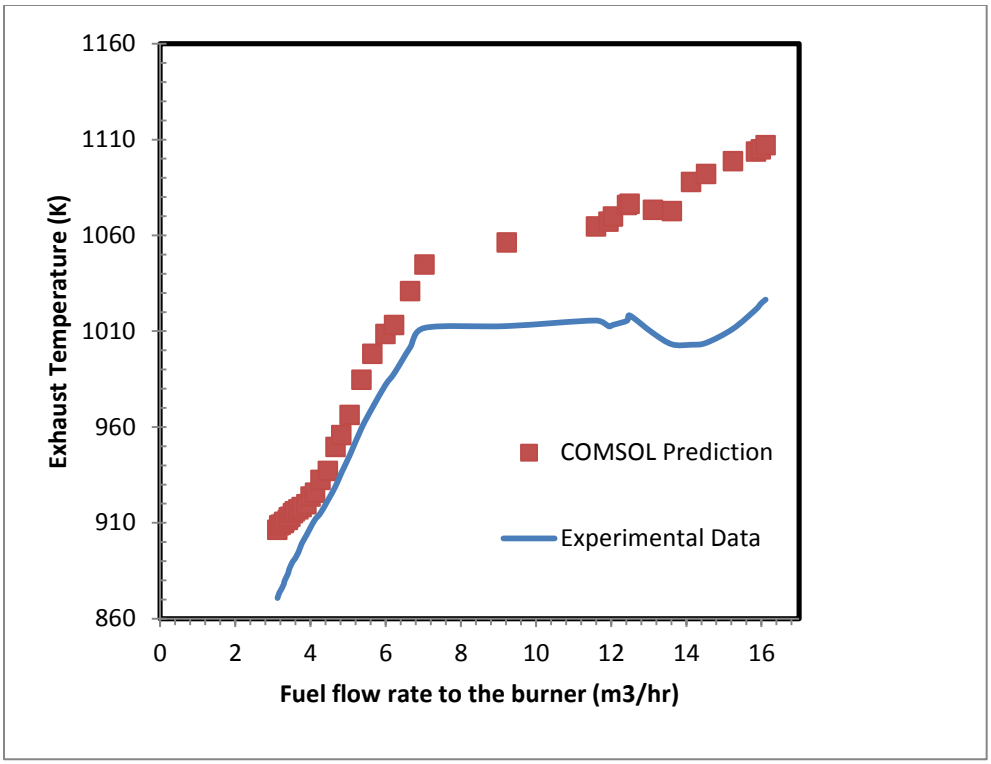

Figure 30: Comparative analysis for the validation of the COMSOL™ model **

**Comparison of the data, for given volumetric flow rates, can be seen in table * in the Appendix.

The model agrees relatively well with the measured data. Figure 30 shows the experimental exhaust temperature compared to the predicted exhaust temperatures as determined by COMSOL™ model at similar air-fuel flow rates. The temperature difference between experimental and COMSOL™ exhaust temperature was calculated, on average, to be about 52K. This difference is likely due to a greater rate of heat loss than predicted by the COMSOL simulation.

It can be seen in figure 30, that at a fuel flow rate of approximately 12.5m^3/hr, there is a dip in exhaust temperature for the measured data. This is due to a leak in the fuel inlet to the burner. The information about the leak was provided by Adam Tuck's colleague when the data was provided. This leak was not incorporated during the data validation, as there was no information provided about how much of inlet fuel was leaking [5]. Over the given time, the pattern of the COMSOL™ modelled data matches the measured data of NRC-IFCI, even after the leak in the fuel inlet.

It can be concluded that this COMSOL^{TM} model provides a good understanding and verification of non-premixed fuel- air combustion in a ceramic porous burner for a 1kW diesel fuelled SOFC system. It should be noted that this analysis focused more on the feeds being non-premixed and variation in the volumetric flow rates of the air and fuel feed. For the optimization of the burner performance, design variables such as porosity, pore length should be varied and analyzed.

4.4 Works Cited

[1]Tuck, A. (2011-2013). Personal Communication. (Y. Khan, Interviewer)

[2]Kennedy, L. (2002). Filtration Combustion of a methane wave in air for oxygen-enriched and oxygen depleted environments. Proceedings of the Combustion Institute, Volume 29, 835-841.

[3]Mohamad, A. A. (2005). Combustion in porous media: fundementals and applications. In Transport phenomena in porous media III (pp. 287-304).

[4] Bibrzycki, J., & Poinsot, T. (n.d.). Reduced chemical kinetic mechanisms for methane combustion in O2/N2 AND O2/CO2 atmosphere. 1-24.

[5]Petit, C. (2013, June). Personal Communication. (Y. Khan, Interviewer)

[6] Poling, B. E., & Prausnitz, J. W. (2000). The Properties of Gases and Liquids, 5th Ediiton. New York: McGraw-Hill.

[7]Smith, G., & Golden, D. (n.d.). GRIMECH 3.0. Retrieved December 2012, from http://www.me.berkeley.edu/gri_mech/

[8]Wilke, C. R., & Fairbanks, C. F. (1950). Diffusion Co-efficient in Multi-Component Gas Mixtures. In Industrial and Engineering Chemistry (p. 471). Berkeley.

[9]Zircar Ceramics properties - ZAL-15. (n.d.). Retrieved February 2013, from Zircar Ceramics: http://www.zircarceramics.com/pages/rigidmaterials/specs/zal15.htm

Chapter 5

Conclusions and Recommendations

5.1 Conclusion:

The focus of this thesis was the system design and component characterization for a 1kW diesel fuelled SOFC system. The first objective was to develop a steady-state process simulation of a small scale diesel-fuelled SOFC system. This process simulation provided a tool for analyzing the performance of a fuel cell system that was fueled by processing conventional diesel to produce 1kW power output as electricity at a greater efficiency and, consequently, with a reduction in GHG emissions, when compared to a conventional small-scale combustion engine generator. The system has been modeled using the simulation software package, VMGSim^{TM}, and utilized a recently developed fuel cell unit operation. This preprogrammed unit operation was in effect being tested in this simulation as well. The unit operation calculated the stack efficiency; power output and methane conversion by internal reforming in the fuel cell anode, but the requirement of precise internal dimensions and specific material properties of the fuel cell stack made its implementation somewhat cumbersome.

For the base case scenario, the oxygen to carbon ratio for auto-thermal reforming was set at 0.31 to achieve 1 kW net power output; the mass flow rate of diesel feed of 0.26 kg/hr was required. The fuel utilization was 85% for this case and the air utilization was 28%.

The fuel cell efficiency based on the lower heating value of the reformate to the anode was determined to be 62%. The gross power output of the fuel cell was 1200W, with the overall system efficiency calculated to be 41%, which is good agreement with reported values in literature. From this simulation it was determined that the afterburner produced 780W of thermal energy, which could be used to vaporize diesel

and water feed. The parasitic load, in this case, comprises of energy provided to pumps, blowers and compressors.

A sensitivity analysis of key operating and design variables was carried out in order to investigate their influence on the net system efficiency, exhaust temperature and stack efficiency. S/C ratio and O/C ratio were varied and following observation were concluded.

- The system exhaust temperature was most sensitive to the S /C ratio, because a greater heat of vaporization was required at higher ratios to generate steam.
- An increase in S/C or O/C ratio of the system, initially results in an increase of net system and stack efficiency, followed by a decrease in efficiencies.
- For highest system efficiencies of 43% and 41%, the O/C ratio was 0.33 and the S/C ratio was approximately 2.75.

In the second part of the thesis, tail-gas burner was modelled using COMSOL™. The model was based on a design developed by Adam Tuck of the NRC-IFCI. Anode and cathode exhausts from the fuel cell stacks were fed separately to the burner and the flame was stabilized using a porous ceramic cup. The anode exhaust, fuel stream and the cathode exhaust, depleted air stream, were not premixed before entering the burner. This proved to be particularly challenging as there are very few examples of burners based on this configuration in use and very limited published analysis and performance data for this configuration.

A simplified kinetic model for the combustion process occurring in the burner at the ceramic burner was utilized. This less complex combustion model was required based on the COMSOL™ limitations. Three metrics were used to evaluate the model predictions: i) velocity profile, ii) temperature profile, and iii) concentration profile.

As mentioned above, the non-premixed feed of fuel and air enters the ceramic burner and the combustion reaction occurs near the outer boundary of the ceramic porous media, as advised by Adam Tuck. According to the results gathered for the base case scenario, the inlet velocities are set at 10 m/s based on the volumetric flow rate required for an 800 W burner. It calculated that the velocity of the flow through the porous media is very low, on average, and was found to be 0.05m/s. The model predicts a significant temperature maximum of approximately 1250K at the outer boundary of the porous region and virtually all the fuel is converted in that zone. The outlet temperature was estimated to be 960K. The temperature of the combustion surface is approximately 290K higher than the exit temperature. The temperature difference is accounted by the significant heat losses via radiative heat transfer from the region of high temperature to the outer wall as well as heat loss through conduction to the flanges and mounting bracket.

The COMSOL™ model was used to test the impact of lean and rich fuel mixtures and its effects on the outlet exhaust temperature. Variations of this nature would be expected during transient in the load on the SOFC stack. The results show that as the oxygen concentration is increased beyond stoichiometric the outlet exhaust temperature decreases significantly. Maintaining the fuel-air feed ratio near stoichiometric will provide higher quality heat for the overall system. During operating transients when excess air flow is used to regulate stack temperature it might be preferable to divert some of the cathode exhaust from the burner to avoid this scenario.

When the volumetric flow rate of the fuel into the burner is increased, it results in an overall increase in the outlet exhaust temperature as would be expected.

When the COMSOL™ model was reconfigured for a premixed feed, of fuel and air, entering the system from the fuel inlet, of the outlet temperature was similar to that for the non-premixed feed simulation. There is no inherent problem in terms of heating capacity at steady-state for using a non-premixed feed with this specific porous ceramic tail-gas burner. Other factors, however, such as startup and purging at shut down might influence the choice of whether a premixed feed would be more convenient.

For comparison of results, this model was matched to the results collected for a 1kW syngas SOFC system tail-gas burner at NRC-IFCI. The results of the model agreed reasonably well with the experimental results provided from the NRC-IFCI testing.

5.2 Recommendations and Future Work:

The simulation of the diesel-fuelled SOFC system was carried out at an arbitrary set of conditions based on steady-state theoretical process calculations and typical values from the literature. The system simulation would be more useful if it were validated against experimental data for an actual operating system. Key variables such as fuel and air utilization should be systematically varied and the prediction of the simulation compared to the response of the actual system. The use of the preprogrammed fuel cell unit operation in VMGSim™, limited the adjustment of certain variables in the system model. Further testing could be done with technical consultation from VMGSim™.

The system design and the tail-gas burner modelling were done out at steady state conditions and do not take into account the system start-up and shut down. A transient model would help in evaluating the impact of transients on overall system performance. For the ceramic porous burner, the model should be further evaluated by systematically varying the key operating variables. The ceramic burner was validated using experimental data for a syngas burner with hydrogen as the fuel inlet. For a more meaningful validation, a ceramic tail-gas burner using a mixture of methane, hydrogen and carbon monoxide as fuel should be tested and compared.

Appendix A.1

Table 17: Additional Fuel cell stack setup information

System Settings							
				H2 Split			
StoC	2.25			anodein			
Air Utilz (%)	0.25			Total Flow Rate		[gmol/s]	0.03
O2toC	0.312			H2 Mol Fraction			0.32
				CO Flow Rate		[gmol/s]	0
				H2 Equ Flow Rate			9.52E-03
				H2 Split		meth 1	0.8
Cell Settings						meth 2	0.8
Faraday Constant			[s.A/mol]	96485			
Current			[A]	15			
Cell area			[cm2]	100			
Number of cells in series				98			
Number of cells in parallel				1			
Total cell count				98			

Table 18: Other results for initial fuel cell simulation in VMGSim

Current density		[A/cm2]	0.15	[A/m2]	1500	
Cell voltage		[V/cell]	0.693			
Stack voltage		[V]	67.91			
Stack power		[W]	1019			
O2 consumed		[gmol/s]	0.003809	0.013712	[kgmol/hr]	
O2 feed composition			0.21			
H2 consumed		[gmol/s]	0.007618	0.027424	[kgmol/hr]	

Some of the graphs produced by the fuel cell unit operation in VMGSim:

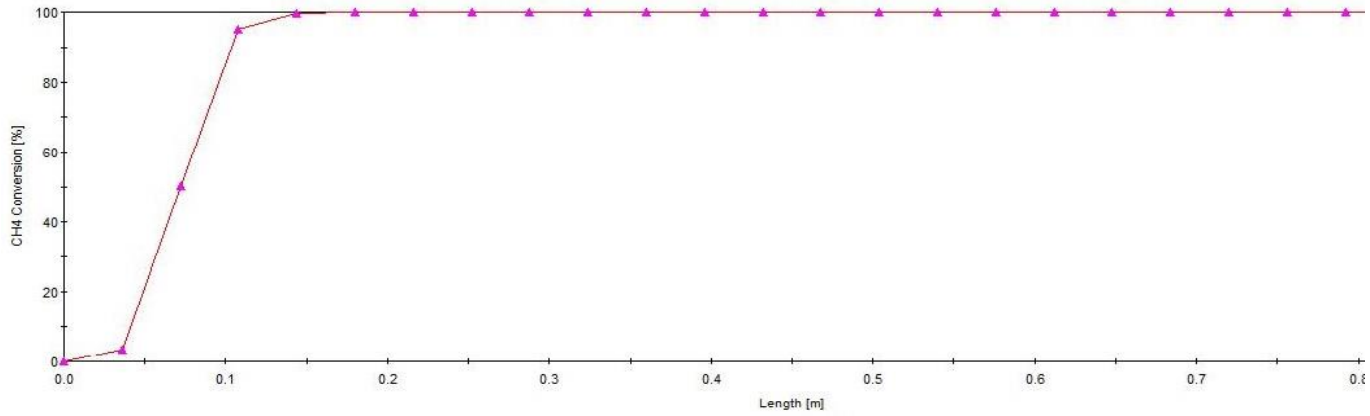

Figure 31: Methane conversion in the fuel cell stack

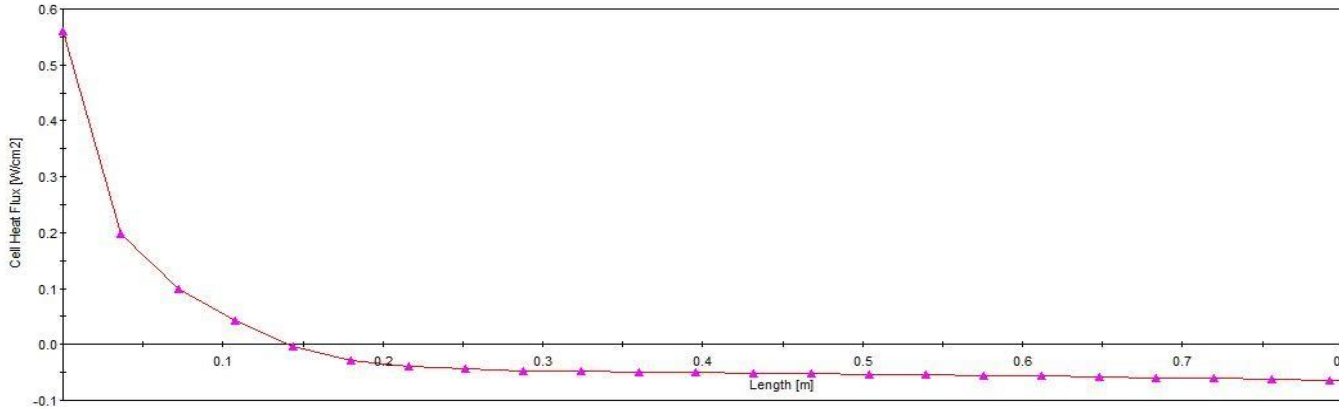

Figure 32: Cell Heat flux in the fuel cell stack

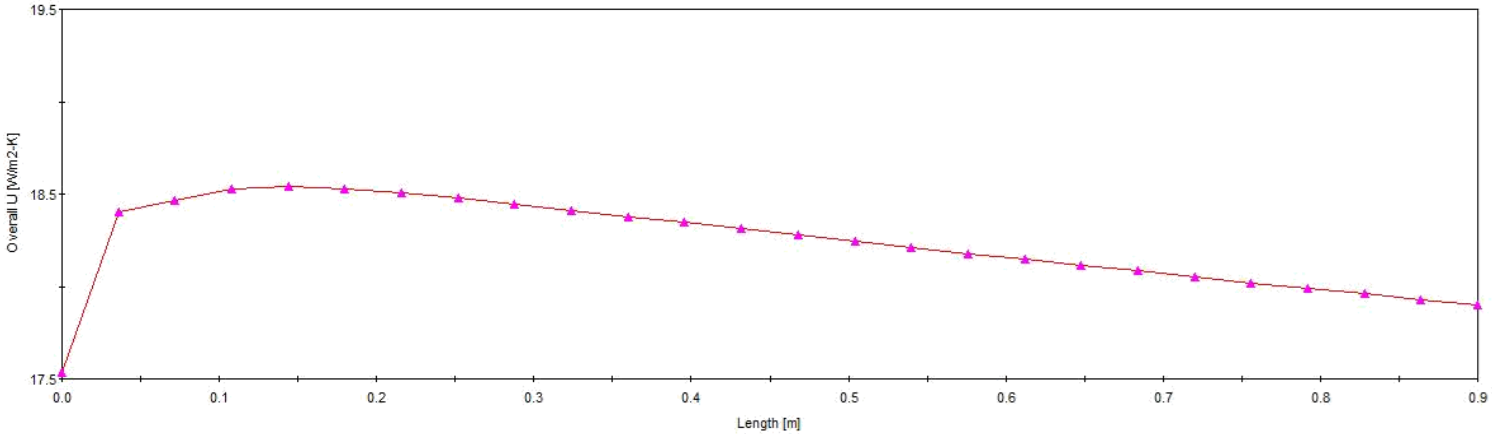

Figure 33: Overall Heat Transfer co-efficient (U)

Appendix A.2

Table 19: Validation Data for the afterburner (provided by NRC-IFCI)

Time	TE-420_AnodeGas_InletTemp (K)	TE-422_CathodGas_InletTemp (K)	TE-453_Hotbox_Temp (K)	Air Act	Fuel Act	Afterburner Act	TE-452_AfterBurner_ExitTemp (deg)	TE-452_AfterBurner_ExitTemp (K)	COMSOL Afterburner_ExitTemp (K)
16:38	410.9	410.78	682.14	136	5.02	960	597.63	870.78	906.33
16:39	412.83	412.72	683.39	138	5.12	960	600.25	873.4	908.6
16:40	414.63	414.53	684.59	141	5.21	961	601.83	874.98	908.91
16:41	416.52	416.4	685.83	145	5.4	961	604.79	877.94	909.76
16:42	418.38	418.26	687.06	147	5.41	957	606.53	879.68	910.5
16:43	420.62	420.52	688.31	149	5.65	959	610.3	883.45	911.48
16:44	422.53	422.42	689.51	154	5.68	954	612.11	885.26	912.78
16:45	424.4	424.29	690.67	156	5.79	961	614.18	887.33	913.12
16:46	426.39	426.3	691.86	157	5.96	960	616.93	890.08	915.04
16:47	428.41	428.31	693.1	161	6	959	618.03	891.18	915.95
16:48	430.66	430.55	694.27	165	6.28	963	621.71	894.86	916.95

16:50	434.81	434.7	696.7	170	6.43	963	625.92	899.07	918.2
16:52	439.16	439.06	699.14	200	6.7	962	630.4	903.55	919.6
16:54	443.36	443.26	701.6	182	6.89	960	634.54	907.69	923.6
16:56	447.95	447.83	704.07	200	7.17	961	638.62	911.77	925.704
16:58	452.29	452.2	706.6	194	7.45	961	641.95	915.1	932.4
17:01	459.4	459.29	710.35	200	7.82	959	648.71	921.86	937.1
17:04	466.38	466.27	713.94	200	8.16	958	655.85	929	949.56
17:07	473.46	473.36	717.47	200	8.42	962	663.02	936.17	955.78
17:11	482.67	482.57	722.27	199	8.8	955	672.2	945.35	966.3
17:16	494.36	494.23	728.49	199	9.3	957	686.35	959.5	984.63
17:21	505.81	505.69	734.82	200	9.73	958	696.99	970.14	998.169
17:26	517.19	517.08	741.31	199	10.29	961	708.93	982.08	1008.57
17:29	524	523.88	745.23	200	10.67	958	714.89	988.04	1013.23
17:35	537.47	537.34	752.47	200	11.3	961	728.35	1001.5	1030.865
17:40	548.86	548.73	758.55	200	11.91	961	738.58	1011.73	1044.69

17:41	556.31	556.21	759.84	200	11.89	975	739.53	1012.68	1056.29
17:42	563.9	563.83	761.35	199	12.22	982	742.43	1015.58	1064.53
17:45	580.35	580.2	767.01	200	12.11	971	739.43	1012.58	1067.16
17:46	584.72	584.61	768.81	200	12.19	972	740.15	1013.3	1069.8
17:52	605.6	605.49	778.16	200	12.07	981	742.4	1015.55	1075.8
17:54	616.85	616.83	780.94	191	11.73	982	745.09	1018.24	1076.38
17:55	655.82	655.74	782.8	199	11.39	966	735.84	1008.99	1073.34
17:56	665.95	665.81	785.54	198	11.99	949	730.01	1003.16	1072.68
17:57	671.67	671.55	787.81	197	12.75	940	729.81	1002.96	1087.75
17:58	676.59	676.48	789.67	198	13.34	938	730.79	1003.94	1092.02
18:01	689.03	688.9	794.19	199	14.19	944	738.11	1011.26	1098.71
18:05	702.37	702.24	800.08	200	14.8	959	748.4	1021.55	1103.6
18:06	705.37	705.25	801.64	200	14.9	962	751.21	1024.36	1104.9
18:07	708.19	708.06	803.22	200	15.02	966	753.35	1026.5	1106.934